JOURNAL OF PETROLOGY | VOLUME 45 | NUMBER 11 | PAGES 2225–2259 | 2004 | doi:10.1093/petrology/egh054

Experimental Petrology of the Kiglapait Intrusion: Cotectic Trace for the Lower Zone at 5 kbar in Graphite

S. A. MORSE[1]*, J. B. BRADY[2] AND B. A. SPORLEDER[3]

[1]DEPARTMENT OF GEOSCIENCES, UNIVERSITY OF MASSACHUSETTS, AMHERST, MA 01003-9297, USA

[2]DEPARTMENT OF GEOLOGY, SMITH COLLEGE, NORTHAMPTON, MA 01063, USA

[3]DEPARTMENT OF GEOLOGICAL SCIENCES, BINGHAMTON UNIVERSITY, BINGHAMTON, NY 13902, USA

RECEIVED OCTOBER 29, 2002; ACCEPTED JUNE 28, 2004
ADVANCE ACCESS PUBLICATION SEPTEMBER 16, 2004

The inferred crystallization history of the troctolitic Lower Zone of the Kiglapait Intrusion in Labrador is tested by melting mineral mixtures from the intrusion, made to yield the observed crystal compositions on the cotectic trace of liquid, plagioclase, and olivine. Melting experiments were made in a piston-cylinder apparatus, using graphite capsules at 5 kbar. Lower Zone assemblages crystallized from 1245°C, 5% normative augite in the liquid, to 1203°C, 24% normative augite in the liquid at saturation with augite crystals. This transit is consistent with modal data and the large volume of the Lower Zone. The 1245°C cotectic composition matches the average Inner Border Zone composition. Quenched troctolitic liquid from the Upper Border Zone, and others from nearby Newark Island, plot on or near our experimental cotectic, supporting a common fractionation history. Olivine–plagioclase intergrowths from cotectic troctolitic melt show mosaic textures reflecting the differing barriers to nucleation of these two phases. The linear partitioning of X_{Ab} in plagioclase–melt yields an intercept constant $K_D = 0{\cdot}524$ for these mafic melts. Observed subsolidus exchange of Ca between plagioclase and olivine elucidates the loss of Ca from plutonic olivines. The bulk composition of the intrusion is revised downward in Fo and An.

KEY WORDS: *experimental; olivine; plagioclase; Kiglapait; partitioning*

LIST OF ABBREVIATIONS

AP, MT, IL, OR, AB, AN, DI, HY, OL, FO, NE, Q, FSP, AUG: (Oxygen) Normative components
Ap, Aug, Ilm, Ol, Pl: Phases
Ab, An, Di, Fa, Fo, Or, Wo: Phase components; also ternary endmembers
BSE: Back-scattered electron
CaTs: Calcium Tschermak's component, $CaAlAlSiO_6$
D: Partition coefficient
f: Fugacity
F_L: Fraction of the system present as liquid = 1 − (PCS/100)
FMQ: Fayalite = magnetite + quartz buffer
IBZ: Inner Border Zone
IW: Iron = wüstite buffer
kbar: kilobar, 10^8 pascal
K_D: Exchange coefficient
KI: Kiglapait Intrusion
L: Liquid phase
LLD: Liquid line of descent
Ma: Mega-annum, age
Myr: Mega-year, time
OLHY: Normative OL + HY
OLRAT: The ratio OLHY/(OLHY + AUG)
P: Pressure
P: Phosphorus
PCS: Percent solidified (volume)
SMAR: South Margin average composition
T: Temperature, °C
UBZ: Upper Border Zone
WM: Wüstite = magnetite buffer
Wo: Wollastonite component of pyroxene
X: Mole fraction
X_{Mg}: Molar ratio $Mg/(Mg + Fe^{2+})$
X^o_{Mg}, $X_{Mg}(0)$: Initial X_{Mg} before MT is formed in the norm calculation
X: Coordinate, horizontal axis
Y: Coordinate, vertical axis

INTRODUCTION

The precise identification of liquid compositions parental to the rocks of layered intrusions has long been

*Corresponding author. E-mail: tm@geo.umass.edu

an elusive goal of igneous petrology. Even in the case of the Skaergaard Intrusion, the elegant box model and careful volume estimates of Nielsen (2004), when combined with the zone averages of McBirney (1989), contain significant amounts of olivine on the liquidus (as we shall show), inconsistent with the exposed olivine + plagioclase rocks of the Skaergaard Lower Zone. For the much larger volume of the Kiglapait Intrusion (about 3500 km^3, compared to the more tractable 280 $\pm$ 23 km^3 of Nielsen's Skaergaard estimate), a finer scale of sampling was provided by a unified stratigraphic representation of rock compositions and volumes (Morse, 1969, 1979*a*, 1979*b*). These compositions have been summed over their volumes to obtain estimates of liquid compositions (Morse, 1979*b*, 1981*b*). One means of testing the results of any such volumetric summation is to determine experimentally, at pressure, the equilibrium compositions of melts that yield cotectic crystals of the observed natural composition at any given stratigraphic level. Such a test furnishes one answer to an inverse problem: the successful melt compositions could have given rise to the observed rocks. That test is the goal of the research reported here.

A study of olivine compositions in the Kiglapait Intrusion (Morse, 1996) was undertaken because the well known partitioning of Fe–Mg between olivine and liquid could give an objective constraint on the liquid compositions to compare with the summation model calculated from the chemical compositions of the rocks (Morse, 1981*b*). The summation liquid is much too Mg-rich to account for the observed olivine compositions in the rocks of the intrusion. This result led to the conviction that the same problem would also arise for the plagioclase composition. These problems were clearly identified by Blundy (1997), who concluded that the liquid parental to the actual Kiglapait rocks must have been significantly more evolved (less refractory) in terms of AN and FO than the chilled margin sample. That sentiment is the foundation stone of the present investigation, whose purpose it is to ask: What plausible cotectic liquids could yield the observed An and Fo contents of the Lower Zone rocks, and at what temperatures? Where does the cotectic trace lie in the ternary? How far away from the starting point is the saturation point with augite?

To answer these questions, we made mixtures of separated Kiglapait minerals that, when melted just below the liquidus, would yield liquids on or near the cotectic condition *L*(Ol, Pl), and crystallize plagioclase and olivine having the compositions observed in the intrusion. Then, by incrementally adding an augite component along the cotectic, we eventually found the saturation point with augite crystals, defining the boundary between the Lower and Upper Zones of the intrusion. Our emphasis was on producing liquids of the appropriate composition, for which the crystal compositions were found by partitioning relations made on longer runs to achieve compositional equilibrium.

Experiments at pressure are, of course, relevant to the natural intrusive setting of a layered intrusion, but they have added advantages. Graphite containers tend to stabilize the oxygen fugacity near that of the input charge, and the crystals produced near the liquidus tend to be large, euhedral and unzoned. They are, therefore, easy to characterize by electron microprobe, and to interpret texturally. Our experiments were conducted in the Experimental Petrology Laboratory at Smith College, Northampton, MA. This study is an outgrowth of a Masters thesis by Sporleder (1998), which contains further details. We begin by assuming that the summation liquid composition of Morse (1981*b*) is an appropriate starting point in terms of the phase abundances, but not in terms of normative plagioclase and olivine compositions.

PREVIOUS WORK

Field relations

The Kiglapait Intrusion was emplaced into Archean migmatites, Proterozoic supracrustal rocks and anorthosites of the Nain Plutonic Suite (NPS), Labrador (Ryan, 1990) at 1307 $\pm$ 2 Ma (age reviewed in Morse, 1996, p. 1038; Yu & Morse, 1992). It is the youngest dated member of the NPS, and one of a suite of Proterozoic troctolitic intrusions that typically cut anorthosite, both in Labrador and elsewhere (Scoates & Mitchell, 2000). The contact rocks are dry granulites (Berg, 1977) previously heated by emplacement of anorthosite (Yu & Morse, 1992). The country rocks to the north-west and north are metamorphosed sedimentary rocks of the Aphebian Snyder Group (Speer, 1978) lying unconformably on Archean gneisses and overlain by the Falls Brook Group of mafic and ultramafic igneous rocks, banded iron formation, calc-silicate rocks and pyroxene paragranulite (Schuh, 1981). The southern and western contact rocks and roof rocks are anorthosite, and nearby to the west is the large, troctolitic Hettasch Intrusion (Berg, 1980; Berg *et al.*, 1994). The emplacement pressure of the Kiglapait Intrusion was near 2·5 kbar (Berg, 1977, 1979, 1980; Berg & Docka, 1983). The present experimental study was conducted at 5 kbar (500 MPa) in view of the difficulty of maintaining long runs at lower pressures in the piston-cylinder apparatus.

The history of studies on the bowl-shaped Kiglapait Intrusion was reviewed, with map, cross-section and stratigraphic column, by Morse (1996). The initial depth of the magma body is estimated at nearly 9 km, almost all of which is preserved at the center, but much of which is lost in the presumed eroded wings (Morse, 1969). The former Outer Border Zone (Morse, 1969) is now equated with the Falls Brook Group, which may contain sills of

Kiglapait material (Morse, 1979*a*). An Inner Border Zone (IBZ) of medium- to very coarse-grained olivine gabbro surrounds and underlies the entire layered series and grades upward into troctolites of the Lower Zone. Some finer-grained samples of this unit have been analyzed and may nearly represent the magma composition.

A large Lower Zone (LZ) of troctolite is overlain by an Upper Zone (UZ) that varies from olivine gabbro at the base to fayalite–mesoperthite ferrosyenite at the top. A fine-grained Upper Border Zone (UBZ) contains the same stratigraphic sequence inverted, ranging from Mg-rich troctolite at the highest elevation to closure with ferrosyenite at the base (Morse, 1990). Foundered layers of the same UBZ lithology occur in the northern part of the Upper Zone (Morse, 1969). The UBZ contains an elevated content of red biotite and more products of trapped liquid than the layered series.

Except for an olivine-rich basal Lower Zone and some inverted mineral variation near the base, attributed to influx of fresh or fractionated magma, the intrusion is provisionally taken to represent a closed system. Stratigraphic height in the intrusion is represented by volume percent solidified (PCS), determined by numerical integration over the inferred shape of the intrusion (Morse, 1969). The inferred shape is consistent with gravity data for the intrusion (Stephenson & Thomas, 1978). Compositional parameters are plotted against PCS, commonly as represented by the fraction of liquid remaining, $F_L = 1 - (PCS/100)$ (Morse, 1979*a*). Subject to the closed-system assumption, the value of any extensive (mass-dependent) parameter in the liquid at any value of PCS is obtained by summation from the top down under a rock composition curve drawn through the data for the parameter concerned (Morse, 1979*a*).

A spike in the concentration of Ni in olivine at 15 ± 5 PCS (Morse *et al.*, 1991) is defined by values of 620–830 ppm Ni over a background of ~490 ppm. This spike furnishes the only known direct evidence of recharge with fresh magma. However, the reverse mineral variation of olivine and plagioclase compositions runs to as high as 30 PCS. These trends are due, in part, to crystallization of trapped liquid, decreasing with PCS, and, in part, perhaps, to the addition of fractionated magma.

The upward stratigraphic variation of cumulus mineralogy begins with olivine plus plagioclase in the Lower Zone, joined by augite at the base of the Upper Zone (84 PCS), by Fe–Ti oxide at 88·6 PCS, by sulfide, essentially troilite, at 91 PCS, by apatite at 94 PCS and by feldspar that grades to antiperthite at 96 PCS and to mesoperthite at 99·65 PCS.

In addition to cumulus olivine and plagioclase, the Lower Zone contains interstitial traces of excluded components that report as the minerals augite, Fe–Ti oxides, sulfide, apatite, and scarce rims of hypersthene, brown hornblende and red biotite. When the modal abundance of these excluded minerals is divided by their calculated abundance in the modal summation liquid, the results give consistent estimates of the residual porosity, which is found to decrease systematically with stratigraphic height from 0·14 at the fictive beginning of crystallization to 0·03 at 80 PCS (Morse, 1979*b*). The residual porosity, representing trapped liquid that fractionated in place, was found to be correlated with the range of An determined in grain mounts of plagioclase, so the variability of An can be used as a proxy for residual porosity (Morse, 1979*b*). From this relation, it was possible to quantify the amount of trapped liquid in the UBZ, and, hence, to find a complete correlation between calculated PCS levels in the UBZ, using the maximum (core) value of An in plagioclase, compared with the average value of An in the layered series (Morse & Allison, 1986).

The phases augite, oxide minerals and sulfide do not appear abruptly in the Upper Zone stratigraphy, but, instead, their abundance increases regularly to a peak, then falls back to a sustained but decreasing trend with increasing PCS. By contrast, apatite appears abruptly at $94 \pm 0{\cdot}3$ PCS in all quadrants of the intrusion, just above a massive excess of Fe–Ti oxide minerals, culminating in the Main Ore Band at 93·5 PCS. The incremental appearance and over-production of the three non-abrupt phases was attributed to poor stirring of the large magma body, and the abruptness of the apatite appearance was attributed to a wholesale overturn and mixing of the residual magma consequent upon the precipitation of excess Fe–Ti oxide minerals (Morse, 1979*b*). By balancing areas on the PCS plots, it was calculated that the *equilibrium* saturation of the magma with augite would have occurred at 81 PCS, at a modal ratio of olivine/(olivine + clinopyroxene) equal to 0·36 (Morse, 1979*b*, fig. 21). Testing this estimate is one target of our investigation.

Volatiles and intensive parameters

Of further importance to the present investigation, the water content was estimated at 68 ppm, apatite is F-rich and trace biotite is a fluorine oxybiotite (Huntington, 1979). Oxygen isotopes are those of normal igneous rocks, and, stratigraphically, they reflect a secular change, consistent with the observed mineralogy and calculated fractionation factors (Kalamarides, 1984, 1986).

The intensive parameters of oxygen and silica activities are well constrained from a study of Fe–Ti oxide minerals and silicate compositions (Morse, 1980). In this study, it was deduced that the Lower Zone liquid path ranged from the WM buffer at 0 PCS to about halfway towards the FMQ buffer (at $\Delta_{FMQ} \sim -0{\cdot}4$ log units) when titanomagnetite first precipitated at 86 PCS. The corresponding average silica activity for the Lower Zone was estimated at $a_{SiO_2} = 0{\cdot}55 \pm 0{\cdot}007$, compared with 0·7 for

the Skaergaard Intrusion (Morse, 1980, p. 712; Morse, 1990, p. 242). Because the oxygen and silica activities are coupled in this system (Morse, 1980), the oxygen fugacity specifies the silica activity, and vice versa. The results of these calculations are consistent with the absence of cumulus orthopyroxene, the consequently Wo-rich compositions of the augite series (Morse & Ross, 2004), and with the undersaturated, ferric-iron-free composition of pargasitic amphibole rims (Morse, 1979*b*). An extended discussion of the contrasting intensive parameters in the Kiglapait and Skaergaard intrusions is given by Morse (1990).

Composition estimates

The widely scattered modal data of Morse (1979*b*), constrained by the measurements of rock density (Morse, 1979*a*), yielded a calculated bulk composition for the intrusion, and a summation liquid path expressed in terms of the volumetric mode. The modal composition is listed in the first column of Table 1, and the modal liquid path, obtained by the summation procedure described in the previous section (see Morse, 1979*b*, p. 594 and footnote), was plotted on the ternary OL–PL–CPX by Morse (1979*b*, figs 21–23). The Lower Zone path of figs 21 and 23 in Morse (1979*b*) furnishes a reference point for the present study, and for the subsequent chemical estimates of liquid compositions obtained by summation.

Because the field truth for the Kiglapait Intrusion is based on rock densities converted to (or supplemented by) petrographic modal data expressed in volume percent, we use oxygen norms to compare chemical data with field data. These oxygen norms (Table 1) are standard calculations (e.g. Morse, 1994) that favor comparison with modal data because oxygen dominates the volume of silicate and oxide minerals. In the ternary compositions, a part of normative HY is assigned to augite (to reflect the natural augite composition of 40% Wo, 10% Hy; Morse and Ross, 2004), and the rest (if any) is assigned to olivine, on the assumption that the excess silica represented by residual HY is within the error of the silica determination. Further details of the ternary calculation, and of the assignment of oxidation state for analyses without ferric iron, are presented in Appendix A.

Samples and analogues

A number of fine-grained rocks in the region also help to constrain estimates of the starting magma composition for the Kiglapait intrusion. The internal consistency of some individual suites suggests that they are reliable samples of initial intrusive magmas. The chilled margin of the troctolitic Hettasch Intrusion (Berg, 1980; Morse, 1981*b*) is a very important clue to the troctolitic nature of the Kiglapait magma, because it is a fine-grained rock chilled against Archean granulites of the Webb Valley Metamorphic Complex (Berg, 1977). The contact zone of this $\sim$200 km^2 intrusion lies approximately along the south-western extension of the Falls Brook Group and the north-west contact of the Kiglapait Intrusion, so the emplacement of the two intrusions may have exploited the same fracture zone in the Earth's crust. The grain size of the chilled rocks is 0·2–3·0 mm (Berg, 1974). The composition estimate—an average of five samples collected over 8 km strike distance along the contact—is shown in column 2 of Table 1. It shares a high feldspar content, low DI, low HY and an olivine content near 20%, with the modal estimate for the Kiglapait Intrusion. It has $An_{55·5}$ and $Fo_{60·2}$.

The large, 400–450 km^2 Jonathon Intrusion (Berg *et al.*, 1994) lies some 10 km south-east of the southern end of the Kiglapait Intrusion and varies upward from leucotroctolite to leuconorite. It has a lengthy, massive, fine-grained (0·2–1·0 mm) chilled margin adjacent to Archean gneisses and granulites. Its composition (column 3 of Table 1) is similar to that of the Hettasch chill, except for a higher value of FO, a lower augite content, lower TiO_2 and K_2O, and higher P_2O_5. These two intrusions flank the Kiglapait Intrusion, and their chilled margin compositions are notable for their consistency and resemblance to the estimated bulk composition of the Kiglapait Intrusion (column 5 of Table 1).

Three rocks of the Kiglapait Inner Border Zone have an average composition (column 4 of Table 1) quite close to the Hettasch average, but with lower Ti, K and P. The normalized ternary augite component of the IBZ is close to 5% AUG. The AN-content of the plagioclase component, $An_{52·7}$, is the next lowest of any in the table.[1]

Column 5 of Table 1 represents the summation from the top down over 48 wet chemical analyses of rocks from the Kiglapait layered series, averaged as guided by the density and modal data of Morse (1979*a*, 1979*b*). Fifteen (31%) of the 48 analyses, evenly distributed along the stratigraphic list, are mildly NE-normative (Morse, 1981*b*, table 3; Morse, 1990, fig. 2). This tendency emphasizes the original interpretation (Morse, 1969) that the Kiglapait magma began and remained at or

[1]The IBZ samples used in the average IBZ composition (Table 1) have not been located on previously published maps. All are from the north-west to northern sector of the intrusion, over a strike distance of 14 km. The reference map is that of Morse (1969). Sample KI 3567 is located in the north-west sector, near the top of the IBZ, just below the floor of the Lower Zone. Sample KI 3708 is located 4·5 km to the north-east, south of Wendy Bay, 100 m above the top of the Outer Border Zone (Falls Brook Group). Sample KI 3623 is located at the top of the IBZ, near the north coast, 9·5 km east of KI 3708, and about 2 km west of the Sally Lake Traverse, depicted in Morse (1979*a*). Map locations and compositional data for samples KI 3567 and KI 3623 are given in Berg (1971).

Table 1: Estimates of Kiglapait composition

	1 MODE		2 HETTAS	3 JONATH	4 IBZAVG	5 KI 1981	6 KI 1986	7 SMAR	8 KI 3763	9 JB94-4
SiO_2			47·94	48·07	47·98	47·46	47·46	49·83	49·78	49·52
TiO_2			1·24	0·68	0·76	0·81	0·81	0·30	0·24	0·33
Al_2O_3			18·95	19·16	18·42	19·46	19·46	19·58	19·76	19·21
Fe_2O_3			1·12	2·09	1·80	1·91	1·04	0·68	0·44	0·91
FeO			10·66	8·90	10·12	9·36	10·14	8·30	8·72	7·38
MnO			0·14	0·13	0·16	0·15	0·15	0·13	0·13	0·17
MgO			7·67	8·48	7·92	8·04	8·04	8·17	8·65	8·03
CaO			8·60	8·60	8·19	9·27	9·27	9·46	8·90	8·86
Na_2O			3·21	3·14	3·43	3·13	3·13	3·10	3·18	3·88
K_2O			0·40	0·30	0·29	0·22	0·22	0·25	0·24	0·96
P_2O_5			0·13	0·30	0·12	0·11	0·11	0·04	0·03	0·07
Total			100·06	99·85	99·20	99·92	99·83	99·84	100·07	99·32
	Vol %					OXYGEN NORMS				
AP	0·21	Ap	0·29	0·65	0·26	0·25	0·25	0·07	0·07	0·11
TIMT	1·09	Mt	1·01	1·87	1·65	1·74	0·97	0·62	0·38	0·82
ILM	0·36	Ilm	1·68	0·92	1·04	1·09	1·09	0·43	0·32	0·43
		Or	2·32	1·73	1·75	1·16	1·16	1·71	1·71	5·77
		Ab	30·12	29·37	32·10	28·94	29·00	28·55	29·08	28·26
FSP	73·20	An	37·54	38·58	35·78	40·12	40·20	39·68	39·81	33·27
AUG	5·74	Di	4·56	2·81	4·38	5·21	5·22	6·21	3·85	9·08
HY	0·36	Hy	2·71	6·80	3·50	2·17	0·43	7·39	6·95	0
OL	18·76	Ol	19·76	17·28	19·55	19·32	21·68	15·34	17·82	18·24
BIOT	0·16	Ne	0	0	0	0	0	0	0	4·04
TROIL	0·05	Q	0	0	0	0	0	0	0	0
PARG	0·07		Total feldspar + olivine + pyroxene, FOP:							
		FOP	97·01	96·57	97·06	96·92	97·69	98·88	99·22	94·62
						TERNARY COMPOSITIONS				
FSP		74·6	72·1	72·2	71·7	72·5	72·0	70·7	71·2	71·7
AUG		5·9	5·6	3·5	5·4	6·5	5·8	7·5	4·7	9·4
OLHY		19·5	22·2	24·4	22·8	21·1	22·2	21·7	24·2	18·9
An		n.d.	55·5	56·8	52·7	58·1	58·1	58·2	57·8	52·4
Fo		n.d.	60·2	67·1	61·9	64·6	61·5	65·2	64·9	68·1

1, Mode constrained by 120 rock densities (Morse, 1979*a*, 1979*b*). 2, Hettasch Intrusion chilled margin, average of five analyses (Morse, 1981*b*). 3, Jonathon Intrusion chilled margin (Berg *et al.*, 1994). 4, Average of three Inner Border Zone analyses (KI 3708, KI 3567, KI 3623; Morse, 1981*b*). 5, Summation over 48 wet chemical analyses constrained by modes (Morse, 1981*b*). 6, Same with modified ferric iron (Nolan & Morse, 1986). 7, Average South Margin composition (Nolan & Morse, 1986). 8, Sample KI 3763 from the South Margin (Nolan & Morse, 1986). 9, Run 94-4 (Pl, Ol, Liq), 1208°C, 1 atm on KI 3763 (Blundy, 1997); Ferrous ratio set at 0·9. Values for Ti, Mn and P carried in from run 94-7. n.d., not determined.

very near critical silica undersaturation throughout its differentiation, and it is consistent with the calculations of silica activity (Morse, 1980, 1990).

A discovery of relatively fine-grained rocks at the southern margin of the Kiglapait Intrusion, against anorthosite, permitted another chance to evaluate the bulk composition of the intrusion (Nolan & Morse, 1986). The texture of these rocks is characterized by $\sim\frac{1}{2}$ mm subrounded olivine grains, larger plagioclase laths and poikilitic augite. No apatite is seen. The average composition of four rocks, labeled 'SMAR', is given in column 7 of Table 1. In this study of the southern margin, it was recognized that the amount of Fe–Ti oxide in the modal study (Morse, 1979*b*) was overestimated and inconsistent with the ferrous/ferric ratio implied by the oxygen fugacity. This discrepancy was then corrected to give a modified summation composition (column 6). One of the SMAR rocks, KI 3768, was used in the present investigation, and its composition will be discussed later. Another, KI 3763, is listed in column 7 of Table 1; its rock powder was furnished to Jon Blundy for a 1 atm study of melting relations and trace element partitioning. This rock has a nearly cotectic *L*(Pl,Ol) composition, and a run with 91% glass co-saturated with Pl + Ol gave the glass composition shown in column 8 (from Blundy, 1997).

All of the SMAR compositions (columns 7–9 in Table 1) are low in Ti and P, and high in K, FO and AN compared with Hettasch, and the IBZ average in columns 2 and 4. (The value of $K_2O = 0{\cdot}96$ in column 8 is clearly aberrant, and probably represents contamination from the furnace; Blundy, 1997.) They are regarded as modified chills, containing some cumulus crystals and lacking significant amounts of excluded components. Drainage of dense rejected solute on a sloping intrusion margin was proposed by Nolan & Morse (1986) to account for this depletion in Ti and P, and the possibility of thermal migration (Lesher & Walker, 1988) was also entertained by Morse (1989), because of the characteristic Soret separation of K from Na. In any event, it is recognized that the SMAR rocks, although useful, are not the best representatives of the bulk composition of the Kiglapait Intrusion.

All of the analyses and estimates of composition in Table 1 have in common a very low modal or normative augite content, consistent with a troctolitic parental magma. The SMAR value (column 6) and the experimental run (column 8) have the highest values of AUG in the ternary normalization. All the others average 5·4% augite, giving a plausible maximum amount of normative augite (AUG) for the beginning of Lower Zone crystallization.

Of interest in the ternary compositions listed at the bottom of Table 1 is the systematic difference between the volume mode and all of the normative entries in terms of the plagioclase/olivine ratio. The mode contains almost 75% plagioclase, in contrast to 72% in the norms, and the olivine is correspondingly higher in the norms. This result illustrates the predictable difference between the volume mode and the oxygen norm of rocks (or melts) rich in plagioclase and olivine. The total of feldspar + olivine + pyroxene in columns 1–6 of Table 1 averages 97%, so the cotectic trace may be plotted in the corresponding ternary with little projection error.

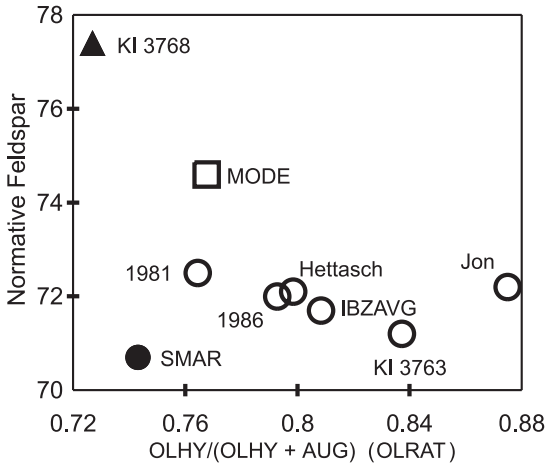

Fig. 1. Compositions related to the Kiglapait Intrusion, from Table 1, and another South Margin sample, KI 3768. The units plotted are those listed under 'Ternary Compositions' at the bottom of Table 1. The average composition of the Inner Border Zone (IBZAVG) and the chilled margin of the Hettasch Intrusion resemble each other closely, but the IBZ average has the lower AN value and is considered the best candidate among those of Table 1 for the composition of the intrusion.

The ternary compositions 1–8 listed in the bottom section of Table 1 are plotted in Fig. 1, where the composition of South Margin sample KI 3768 is also shown. The average of three analyses from the Inner Border Zone (IBZAVG), with AUG = 5·4%, is considered the best candidate for the composition of the Kiglapait Intrusion in all respects except FO-content.

Augite content and ferric iron

The normative ternary AUG-content of the summation liquids in the Lower Zone (Morse, 1981*b*) is plotted against PCS in Fig. 2a. The trend leads back to a value of 5·2% AUG at 0 PCS, which is accepted as a starting point for the cotectic trace in the OLHY–AUG–FSP ternary.

The weight ferrous ratio $FeO/(FeO + Fe_2O_3)$ from the revised KI 1986 composition (Table 1, column 6) is plotted against PCS in Fig. 2b. The value of this ratio was set equal to 0·9 for all calculations of the oxygen norms of electron microprobe analyses of glasses in this study. Although this ratio undoubtedly decreased as the liquid evolved, the effects are minor (Appendix A).

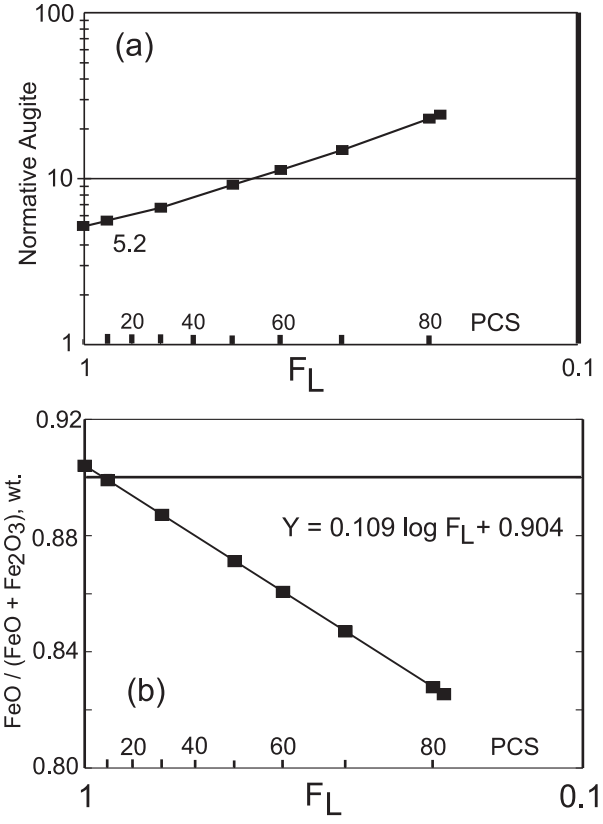

Fig. 2. (a) Normative augite content of the Lower Zone liquid, recalculated as the oxygen norm from summation liquids (Morse, 1981*b*), plotted against the fraction of liquid remaining, F_L, and its complementary percent solidified, PCS. The trend, extrapolated to $F_L = 1{\cdot}0$, gives 5·2% augite at the start of crystallization. (b) Trend of the weight ratio $FeO/(FeO + Fe_2O_3)$ from Nolan & Morse (1986). The value 0·9 was used in the oxygen norm calculation for glasses.

STARTING MATERIALS AND BULK COMPOSITIONS

Purpose and strategy

Starting assumptions and materials

The primary object of this exercise was to find the composition and temperature of the cotectic *L*(Ol,Pl), as a function of AUG-content, from near the OL,PL sideline in the ternary plane OL–PL–AUG, to the saturation point *L*(Ol,Pl,Aug) in a system resembling the composition of the Kiglapait magma. The starting point was chosen at 5·2% AUG, as discussed above. A further constraint was that the liquid compositions along the cotectic should crystallize the olivine and plagioclase compositions observed in the rocks at that stratigraphic level, as calculated from the normative augite content of the liquid using the relationship shown in Fig. 2a. The stratigraphic variation of these mineral compositions is given by

$$\mathrm{An} = 67F_L^{0{\cdot}151} \tag{1}$$

from Morse (1979*a*), and

$$\mathrm{Fo} = 74F_L^{0{\cdot}081} \tag{2}$$

(to 80 PCS only) from Morse (1996). Here and elsewhere, $\mathrm{An} = 100X_{\mathrm{An}}$ and $\mathrm{Fo} = 100X_{\mathrm{Fo}}$, where X is mole fraction.

For this purpose, the reverse composition trends of the basal Lower Zone, representing infilling of the magma chamber, were ignored, and the normal trends of somewhat scattered data were extrapolated to the fictive mineral compositions at the base of the intrusion. This treatment was adopted to provide a model of continuous fractionation from a plausible parental magma that would conform to the mineral composition data above 30 PCS.

These relations may be converted by the linear partitioning equation, described in Appendix B, to the corresponding variations for the liquid, assuming $K_{\mathrm{D}} = 0{\cdot}54$ (see Appendix B) for plagioclase and 0·33 for olivine:

$$\mathrm{AN}^L = 52{\cdot}3F_L^{0{\cdot}208} \tag{3}$$

$$\mathrm{FO}^L = 48{\cdot}4F_L^{0{\cdot}151}. \tag{4}$$

Furthermore, the normative quantity of AUG in the liquid above 10 PCS can be expressed as

$$\mathrm{AUG}^L = 4{\cdot}71F_L^{-0{\cdot}978} \tag{5}$$

in which the exponent *D-1* implies $D = 0{\cdot}022$—very near zero—in keeping with the observation (Morse, 1979*b*: fig. 12) that AUG is an almost perfectly excluded component in the Lower Zone.

We used mixtures of two types of starting materials: a rock composition from a chilled margin and separated minerals from the Kiglapait intrusion. Having on hand a suite of these minerals spanning the feldspar range from An_{66} plagioclase to An_{10} mesoperthite, olivines and augites from Mg_{73} to Mg_0, and apatite and titanomagnetite, we could simulate any proposed Kiglapait liquid. To do this, we chose crystals of the same measured An-content or Mg-ratio as the normative AN-content or Mg-ratio of the intended liquid. The starting materials are listed in Table 2a.

Strategy

Our strategy was first to find the cotectic at an AUG-content of 5·2%, proceeding by trial and error. The location of the *L*(Ol,Pl) cotectic was bracketed at AUG = 5·2% by crystallizing a series of liquids with varying olivine and plagioclase contents in the bulk composition mix. Then, to advance along the cotectic, we formulated new compositions with increased augite component of the appropriate Mg-ratio (Table 2b), and repeated the search for the cotectic. Some of our bulk

Table 2a: Starting materials

Sample:	KI 3768	Fa	Amelia	Ilmen	KI 3367	KI 3369	KI 3345	KI 3243	KI 3347	KI 3188as	KI 4143	KI 3373	KI 3377	KI 3003	KI 3379	KI 1021	KI 3377
Material:	Rock	Olivine	Albite	IL	PL	PL	PL	PL	PL	OL3370	OL	OL	AUG	AUG	AUG	OX	AP
SiO_2	50·79	29·49	68·06	0	55·19	55·74	57·3	57·48	58·33	34·38	33·36	32·83	49·34	49·67	47·74	12·35	0
TiO_2	0·23	0	0	52·66	0·1	0·08	0·07	0·46	0·08	0·02	0·05	0·02	0·7	0·72	1·23	18·32	0
Al_2O_3	21·39	0	20	0	28·31	27·71	26·78	26·91	26·39	0	0	0	1·04	0·90	0·60	2·32	0
Fe_2O_3	0·65	0	0·04	0	0·04	0·03	0·04	0·04	0·07	0	0	0	1·47	1·50	2·15	18·76	0
FeO	6·45	70·51	0	47·34	0·19	0·25	0·2	0·31	0·22	41·74	48·71	50·75	19·82	18·78	22·61	39·38	0
MnO	0·10	0	0	0	0	0·06	0	0	0	0·51	0·76	0·86	0·48	0·39	0·52	0·45	0
MgO	6·31	0	0	0	0·08	0	0·04	0·12	0·06	22·41	17·36	15·23	7·96	6·94	5·33	6·92	0
CaO	9·72	0	0·15	0	9·85	9·55	8·4	8·19	7·52	0·04	0·18	0·08	18·93	21·12	19·56	1·05	55·36
Na_2O	3·62	0	11·49	0	5·23	5·64	5·84	6·09	6·50	0	0	0	0	0·37	0·28	0·41	0
K_2O	0·27	0	0·15	0	0·29	0·34	0·59	0·46	0·59	0	0	0	0·01	0·02	0·01	0·02	0
P_2O_5	0·04	0	0	0	0	0	0	0	0	0	0	0	0	0	0	0·02	42·04
F	0	0	0	0	0	0	0	0	0	0	0	0	0	0	0	0	3·14
Cl	0	0	0	0	0	0	0	0	0	0	0	0	0	0	0	0	0·09
Total	99·57	100·00	99·89	100·00	99·28	99·40	99·26	100·06	99·76	99·10	100·42	99·77	99·75	100·41	100·03	100·00	100·63
X_{Mg}	0·638	0·00							$X_{Fo,\ En}$	0·486	0·384	0·094	0·411	0·392	0·291		
X_{An}	0·577		0·007		0·510	0·483	0·443	0·426	0·390								

Table 2b: Bulk composition formulas (proportions are given in weight fraction)

Bulk comp. Name	KI 3768 Rock	Fa Olivine	Amelia Albite	Ilmen IL	KI 3276 PL	KI 3367 PL	KI 3369 PL	KI 3345 PL	KI 3243 PL	KI 3347 PL	KI 3188as OL3370	KI 4143 OL	KI 3373 OL	KI 3247 AUG	KI 3377 AUG	KI 3003 AUG	KI 3379 AUG	KI 1021 OX	KI 3377 AP	SUM
KI BC96	0·8897	0·0623	0·0356	0·0107															0·0018	1·000
KI BC2 =	0·9434	KI BC96	+								0·0566									1·000
KI BC3 =	0·9091	KI BC96	+								0·0909									1·000
KI R50a						0·0990	0·4950				0·0800	0·2085			0·0814			0·0333	0·0028	1·000
KI R65a							0·0980	0·4838			0·0197	0·2474				0·1130		0·0343	0·0038	1·000
KI 50PCS									0·6300		0·1400		0·0900	0·0300	0·0800			0·0200	0·0100	1·000
KI new50P									0·5756		0·1540		0·0980	0·0350	0·1120			0·0190	0·0070	1·001
KI 60PCS =	0·5000	KI BC2	+	0·5000	KI UZ3															1·000
KI R75a									0·5366			0·1269	0·1087			0·1613	0·0326	0·0258	0·0081	1·000
KI 78PCS										0·5510		0·1860			0·2240			0·0290	0·0100	1·000
KI BC4b =	0·7266	KI BC2	+		0·0867									0·1867						1·000
KI UZ3 =	0·9300	KI UZ2	+							0·0700										1·000
KI UZ2										0·4900			0·2200			0·2900				1·000
KI UZ4 =	0·9300	KI UZ3	+							0·0400			0·0300							1·000

The six formulas with equal signs are to be read as proportions times another bulk composition named, plus whatever else appears in that row.

Table 3: KI–LLD bulk compositions from glass analyses by electron microprobe

Composition	Run	% Glass	SiO_2	TiO_2	Al_2O_3	FeO_T	MnO	MgO	CaO	Na_2O	K_2O	P_2O_5	Total
KI BC96	2K 48·1	100	50·17	0·60	20·05	10·92	0·09	5·92	8·63	3·91	0·25	0·05	100·59
KI BC2	2K 48·2	100	49·28	0·60	19·05	12·50	0·14	6·69	8·21	3·76	0·22	0·09	100·54
KI BC3	2K 48·3	100	48·64	0·66	18·12	13·98	0·16	7·43	7·85	3·51	0·22	0·13	100·70
KI R50a	2K 17·1	100	47·67	0·87	16·58	16·61	0·25	6·19	7·62	3·64	0·18	0·10	99·71
KI R65a	2K 17·2	100	48·03	0·95	15·75	16·47	0·24	5·67	7·72	3·74	0·30	0·19	99·06
KI 50PCS	KI 44·1	99(pl1)	50·29	0·84	16·97	12·80	0·21	5·23	8·13	4·41	0·29	0·35	99·52
KI new50PCS	2K 8·1	100	50·42	0·87	15·67	14·17	0·25	5·94	8·52	4·02	0·28	0·35	100·49
KI 60PCS	2K 8·2	100	51·51	0·43	16·50	13·04	0·19	5·50	9·14	3·80	0·25	0·06	100·42
KI R75a	2K 17·3	100	48·46	0·94	14·46	16·57	0·26	5·22	9·03	3·63	0·25	0·40	99·22
KI 78PCS	2K 8·3	100	50·90	0·75	14·45	14·70	0·24	5·16	9·16	3·79	0·28	0·44	99·87
KI BC4b	KI 43·1	99(pl1)	49·91	0·66	16·58	11·93	0·16	6·56	10·39	3·31	0·21	0·06	99·77
KI UZ3	KI 37·1	94(pl,cpx)	50·98	0·43	14·46	15·14	0·25	4·43	9·71	3·49	0·33	0·06	99·28
KI UZ2	KI 35·1	100	50·14	0·39	13·42	15·70	0·26	4·93	10·32	3·52	0·28	0·01	98·97
KI UZ4	KI 40·1	100	51·19	0·33	14·99	13·95	0·25	4·53	10·02	3·84	0·3	0·01	99·41

compositions are provisional mixtures made on the way to the desired ones. However, these off-composition mixes are useful because they give opportunities for evaluating the effects of composition on the location of the cotectic. Several compositions were purposely made in the plagioclase field in order to acquire new partitioning information for plagioclase.

By using the separated Kiglapait minerals, when plagioclase of appropriate composition for the desired liquid was added, it automatically carried in with it an appropriate amount of K. Similarly, the augite component carried in with it an appropriate amount of alumina, ferric iron and titanium.

Bulk compositions

Bulk compositions were mixed from the starting materials listed in Table 2a, according to proportions listed in Table 2b. They were determined first by calculating the compositions and then by calculating their oxygen norms. Finally, the provisional bulk compositions were melted and analyzed by electron microprobe, and the formula was adjusted if necessary. Six of the mixtures (Table 2b) are made from others by adding other mineral components or other bulk compositions.

The various bulk compositions were finely ground to the approximate range 1–50 μm under acetone using a mullite mortar and pestle, and dried at 120°C overnight to remove adsorbed water. A portion was melted for three hours at 5 kbar in graphite to produce homogeneous glasses, whose composition, determined by electron microprobe analysis, is given in Tables 3 and 4. Grinding ensured a consistent, fine grain size for melting experiments, and helped to promote growth of large crystals of uniform composition. The dried samples were stored in a desiccator.

Because the compositions were made up from Kiglapait minerals, or a rock plus minerals, they resemble the estimated liquid compositions from the estimates (Table 1) of Morse (1981*b*) and Nolan & Morse (1986) in almost all respects. In one respect, however, they fall short. The more augite-rich compositions do not contain as much Ti as in the estimated actual liquids, because it was found that large amounts of Ti and P together (as titanomagnetite and apatite) reacted with the carbon of the capsule to give very high FeO-contents of the liquids (Peterson *et al.*, 1999). Hence, the augite-rich end of the cotectic curve that we find here is appropriate only to a somewhat Ti-depleted analog of the Kiglapait intrusion.

One bulk composition, KI BC4b (Tables 2b, 3 and 4) was made by adding augite component alone to composition KI BC2, without adjusting AN and FO. This was done to study the effects of the mineral compositions on the location of the cotectic, by comparison with the compositions made to match the stratigraphic level of the augite content.

The bulk compositions from Table 4 are plotted with labels in Fig. 3, where data from columns 2 and 4–7 of Table 1 are also shown for comparison. The bulk compositions KI BC2 and KI BC3 flank the critical compositions (open circles) deemed most likely to represent the intrusion composition, and, hence, the initial magma composition.

Artificial cumulates

Sample compositions were also made up as Pl + Ol 'artificial cumulates', to be used for the determination of

Table 4: Oxygen norms of bulk compositions

Composition	Run	AP	MT	IL	OR	AB	AN	DI	HY	OL	SUM	AN/PL	X_{Mg}	X^{o}_{Mg}	FSP	AUG	OLHY	OLRAT
KI BC96	2K 48·1	0·11	1·09	0·80	1·71	35·95	37·27	4·71	2·46	15·90	100·00	50·9	0·552	0·521	76·5	5·8	17·8	0·755
KI BC2	2K 48·2	0·18	1·25	0·81	1·15	35·12	35·59	4·53	2·37	19·00	100·00	50·3	0·544	0·515	73·5	5·6	20·9	0·790
KI BC3	2K 48·3	0·29	1·40	0·92	1·16	33·01	34·34	3·91	4·56	20·41	100·00	51·0	0·544	0·515	70·3	4·8	24·8	0·838
KI R50a	2K 17·1	0·26	1·68	1·22	1·19	35·00	30·14	6·90	1·67	21·95	100·01	46·3	0·453	0·426	68·5	8·5	23·0	0·729
KI R65a	2K 17·2	0·45	1·69	1·34	1·79	35·83	27·28	9·41	3·02	19·18	99·99	43·2	0·436	0·407	67·2	11·7	21·1	0·643
KI 50PCS	KI 44·1	0·73	1·26	1·15	1·75	41·40	26·93	9·84	1·20	15·74	100·00	39·4	0·482	0·449	72·3	11·4	16·3	0·588
KI new50PCS	2K 8·1	0·73	1·41	1·20	1·74	37·80	24·89	12·65	4·47	15·12	100·01	39·7	0·485	0·454	66·7	15·7	17·6	0·529
KI 60PCS	2K 8·2	0·11	1·30	0·60	1·73	35·24	28·20	13·87	8·56	10·40	100·01	44·5	0·481	0·457	66·5	17·0	16·5	0·493
KI R75a	2K 17·3	0·86	1·70	1·35	1·79	35·30	23·82	16·15	2·13	16·90	100·00	40·3	0·413	0·385	63·4	19·0	17·6	0·480
KI 78PCS	2K 8·3	0·92	1·47	1·05	1·76	35·80	22·78	16·72	10·56	8·95	100·01	38·9	0·439	0·411	62·5	20·8	16·7	0·446
KI BC4b	KI 43·1	0·11	1·21	0·93	1·16	30·85	31·32	16·81	5·02	12·59	100·00	50·4	0·554	0·524	64·8	20·6	14·6	0·414
KI UZ3	KI 37·1	0·11	1·53	0·61	2·37	33·16	24·17	19·99	10·66	7·40	100·00	42·2	0·388	0·368	61·1	24·5	14·4	0·370
KI UZ2	KI 35·1	0·00	1·60	0·56	1·80	34·14	21·45	25·15	2·58	12·73	100·00	38·6	0·403	0·383	56·8	28·3	13·0	0·315
KI UZ4	KI 40·1	0·00	1·48	0·44	1·77	36·52	24·15	21·42	3·53	10·75	99·99	39·8	0·411	0·391	63·6	25·4	11·0	0·301

OLRAT is the ratio OLHY/(OLHY + AUG).

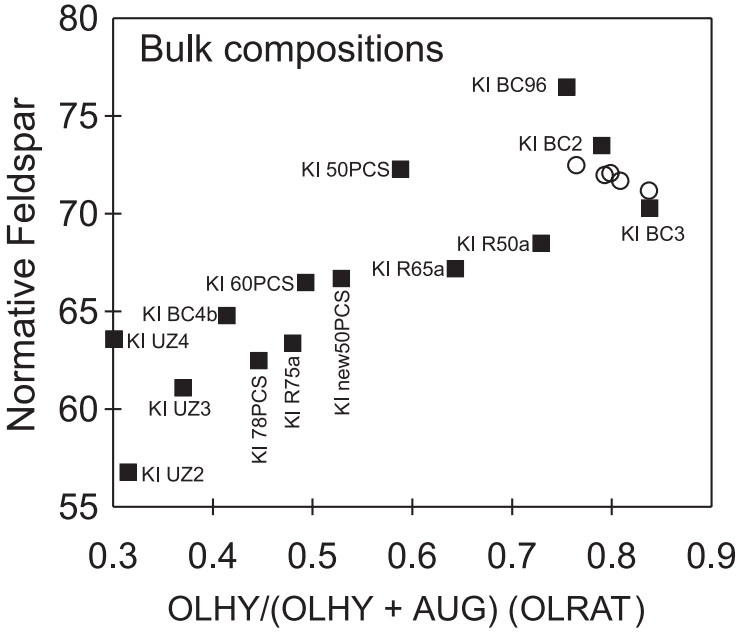

Fig. 3. Normative feldspar content versus the normalized ratio of olivine + hypersthene to olivine + hypersthene + augite in bulk compositions used in this study, from the norms of Table 4. The open circles are those shown in Fig. 1, reproduced here for comparison with the bulk compositions used in experiments. The composition KI BC4b (at 65% feldspar) is made from KI BC2 by adding augite and plagioclase without varying FO or AN, to test the effect of augite independently from the effects of changing mineral compositions. KI BC2, in turn, is made from KI BC96, by adding olivine.

solidus temperatures. The beginning of melting of such a mechanical mixture of the two mineral phases should provide an upper bound to the liquidus temperature of the magma that crystallized these phase compositions. The solidus is an upper bound because the artificial cumulate melts to a liquid on the two-phase join, whereas the natural magma is a complex solution that includes lower-melting components (Morse *et al.*, 1980). The most refractory of these artificial mixtures was composed of olivine KI 3648, $Fo_{71·6}$, and plagioclase KI 3645, $An_{66·1}$,

and was labeled composition KI 4845ac. Its nominal mean stratigraphic level, obtained by inverting equations (1) and (2), is 21 PCS. The solidus temperature of this sample is discussed later in this paper.

Excluded components

Comparisons are shown for the excluded normative components AP, MT, ILM and OR in Fig. 4, for five different stratigraphic levels and for the five bulk compositions as found, compared with the 1986 estimate from Table 1, column 6. The matches for MT and OR are very close, and for AP also close up to the 75 PCS level, but purposely very low at 81 PCS. This difference affords the prospect of testing whether AP by itself might have an appreciable effect on the position of the cotectic, because, if so, there might be a disjunct between the 75 PCS result and the 81 PCS result. The growing deficit in ILM at upper stratigraphic levels is apparent in the figure.

EXPERIMENTAL PROCEDURE

Run assemblies

All experiments were run in a Rockland Research 19 mm (3/4 inch) piston-cylinder apparatus. The end of an 8 mm diameter × 9 mm long graphite rod was drilled with three 1·5 mm diameter × 2·5 mm deep holes, into which were packed the ~7 mg samples of finely ground, dried rock powder. This graphite crucible was covered with a <1 mm graphite lid and placed inside a fired pyrophyllite cup with lid, and this, in turn, was placed inside a graphite furnace, of 1 cm inside diameter, containing MgO spacers below and above the crucible. The furnace was surrounded by a Pyrex tube, a halite sleeve and a lead foil sheath, and then placed in the tungsten carbide core of the cylinder and topped with a brass base plug placed inside a pyrophyllite sleeve. An alumina thermocouple sheath with Type D W-Re thermocouple wires crossed over at the tip was fed through the base plug and upper spacer to rest on the top of the fired pyrophyllite cap, approximately centered above the triangular array of samples.

Samples were pressurized hydraulically to about 120% of the working pressure and then heated in stages with a programmed controller. As the pressure dropped on heating and melting of the sleeves, the ram valve was opened to the reservoir and the pressure kept near the operating pressure of 5 kbar, until, at the run temperature, it was finally brought up to the run pressure in the 'hot piston-in' protocol. Run pressure and temperature were taken as nominal, without correction, based on calibration experiments with gold and sanidine. Heating rates were 100°C/min to $T-90$, then 10°C/min to $T-10$, and 1°C/min to T. The experiments were taken directly to temperature, even for runs below the liquidus, so all melting and crystal growth proceeded from the ground crystalline mixture rather than from glass or melt.

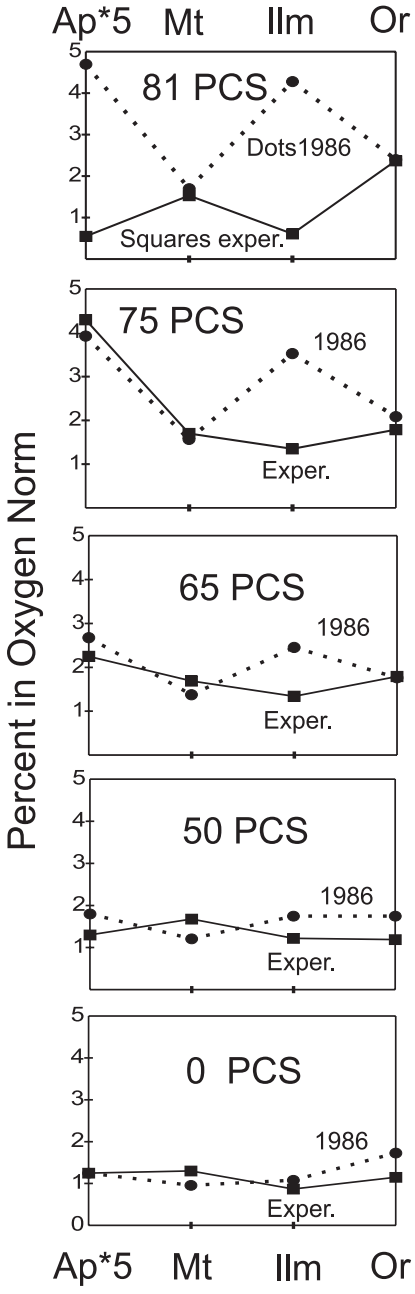

Fig. 4. Comparison of normative AP, MT, ILM and OR found in R-series bulk compositions (Table 4) compared with those sought in the summation model of the intrusion (Morse, 1981*b*; Nolan & Morse, 1986). The experimental values at 0 PCS represent the composition KI BC96 in Table 4. Values for MT and OR are considered well matched, as are those for AP from 0–75 PCS. The experimental ILM values, and the AP value at 81 PCS, are kept low on purpose, to minimize reactions of Ti and P with the graphite crucibles.

Temperatures were controlled to within 1°C, as indicated. Nominal precision of the temperature at the

sample was judged to be ±5°C or better in most cases. Pressure was normally monitored within an indicated range of +50 to −100 bars, with accuracy estimated to be ±300 bars.

Standard run lengths were 3 h for liquidus determinations, and up to 40 h (but generally 8–24 h) for greater equilibration of phases. Runs were quenched by shutting off the power to the furnace. Typical quench times for the first thousand degrees from 1235–1250°C were ∼22 s, or, more generally, -211 ± 2°C $t^{1/2}$ for t in seconds.

Accuracy in temperature was sought in two ways. The midpoint between the sample surface and the thermocouple was centered in the middle of the hot zone, as defined in the calibration study of Watson *et al.* (2002). In addition, many later runs contained a partly crystallizing monitor, either composition KI BC96 or composition 60 PCS, as an internal standard. Runs that appeared normal in terms of expectations and stability yielded a variation of visually estimated percent glass versus temperature near 2·7% glass/deg. The monitors thus allowed correction of questionable run temperatures, and they also allowed extrapolation to the liquidus temperature of any bulk composition. The glass productivity slopes also suggest a liquidus-to-solidus difference of ∼40°C, as a linear approximation. This result means that a sample would spend a maximum of ∼13 min in the partial melt region during a run-up to the liquidus temperature.

Analysis

Recovered run crucibles were mounted in 2·54 cm Epoxy disks and polished for optical examination in reflected light. Phase compositions were determined with the Cameca SX-50 electron microprobe at the University of Massachusetts, using standard procedures based on mineral standards and PAP corrections.

Variance in the experiments

If the bulk composition is known for a closed system of any number of components and any number of phases in equilibrium, then the specification of any two independent variables, extensive or intensive, suffices to determine completely the state of the system. When the two independent variables have been specified, the system is invariant. This is a statement of Duhem's Theorem (e.g. Prigogine & Defay, 1954). Our choice for the independent variables in a given experiment is to specify T and P. The variance is zero in our experiments. Another way of evaluating this invariance is to consider what would happen if it were not so: then, no two experiments on the same bulk composition would yield the same result. The reproducibility of the experiments proclaims the invariance of the system.

EXPERIMENTAL PRODUCTS

Crystalline run products

A list of the run products and experimental conditions is presented in Electronic Appendix 1 (see http://www.petrology.oupjournals.org). The experiments produced a variety of textures (Figs 5–7) depending on temperature, charge composition and run duration. The following descriptions concern only the phases that appeared to be in stable equilibrium at the liquidus. Plagioclase and olivine were the chief crystalline phases observed. Liquidus augite appeared in two runs. Neither apatite nor Fe–Ti oxide crystals were observed. Stable phase equilibrium is inferred from the presence of corner spikes and swallowtails on plagioclase, and of euhedral crystals of olivine and augite. More rarely, internal chemical equilibrium was inferred from the consistent compositions of analyzed grains obtained in long runs (see 'Time studies', below).

In a few samples, micrometer-sized droplets of immiscible melt of metallic iron (presumably Fe–C mixtures from their low liquidus temperatures) were identified from their reflectivity in polished section and microprobe analyses. These occurrences suggest that some of the compositions under some conditions were more reduced than the WM buffer, but not as low as the IW buffer, because the metal is not pure iron.

Most olivine forms euhedral, doubly terminated prisms (Fig. 5a), ranging from long, slender needles to short, squat prisms or wedges. Prisms are 30–100 μm long and 10–70 μm wide. Plagioclase mostly appears as blocky euhedra and laths (Fig. 5b). Euhedra are 20–100 μm long; laths are 20–200 μm long and 5–70 μm wide. Corner swallowtails are ubiquitous and obvious on the smaller laths, but more subdued on larger, blocky laths. Wedge-shaped grains are also present, up to 100 μm long and 40 μm wide. Ubiquitous small plagioclase nuclei, typically 'H'-shaped, evidently formed throughout the duration of the run.

Well-crystallized runs at the cotectic commonly showed euhedral to subophitic intergrowths of olivine around plagioclase. Olivine has a somewhat greater tendency to form hopper crystals and occasional melt inclusions (Fig. 6). In this figure, the swallowtails on small plagioclase crystals are evident.

Augite typically forms equant euhedra (Fig. 7). The larger grains are commonly 50–100 μm long and 40–60 μm wide. The ferrous ratio in this augite (see caption) is 0·89, equivalent to that assumed here for the normative liquid calculation (Appendix A).

Time studies

Plagioclase crystals in these experiments tend to be uniform in composition from grain to grain, and unzoned.

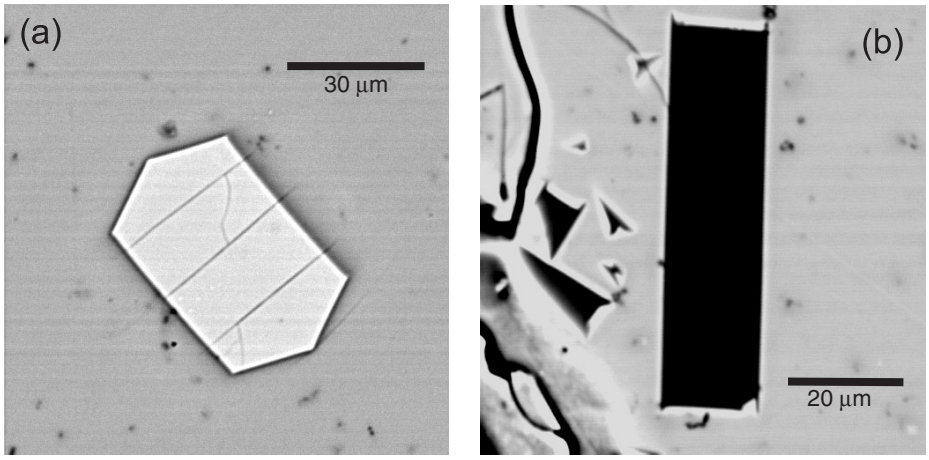

Fig. 5. (a) BSE image of an olivine crystal in a 16·5 h run, KI 20-1 (see Electronic Appendix 1). (b) BSE image of plagioclase crystals grown from composition KI BC96, at 1228°C, just below the liquidus in a 23·3 h run, KI 6a-1. Note swallowtails at corners of the crystals, indicating the mechanism of growth. The large crystal is essentially unzoned.

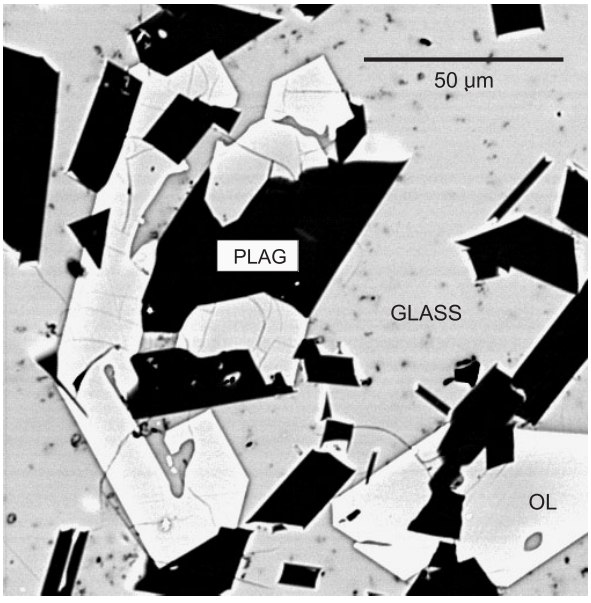

Fig. 6. BSE image of a cotectic assemblage of olivine and plagioclase crystals in glass in a 6·5 h run, KI 29·1, 1200°C, composition KI BC4b.

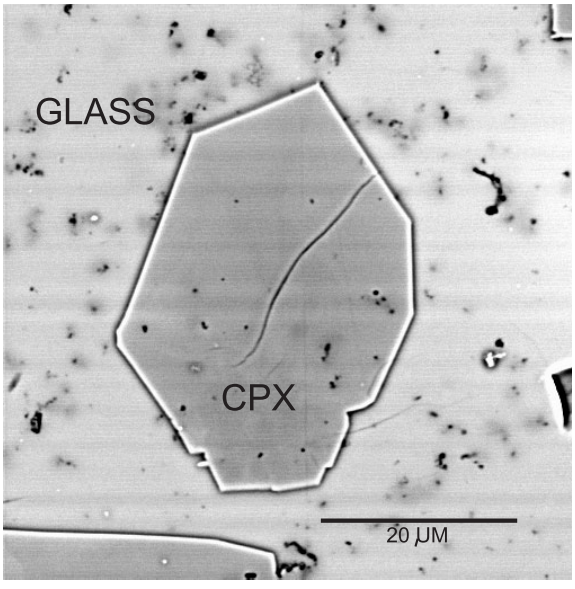

Fig. 7. BSE image of an augite crystal grown for 10 h, Run KI 66-2, 1195°C. The augite composition in this run averages $Wo_{31}En_{48}Fs_{21}$; $100X_{En} = 69{\cdot}4$; CaTs 3·9%, $100Fe^{3+}/(Fe^{3+} + Fe^{2+}) = 10{\cdot}7$. By contrast, the equilibrated natural Kiglapait augites have Wo = 40 and contain no CaTs (Morse & Ross, 2004). Cumulus augites near the base of the Upper Zone have average $100X_{En} = 71$—close to the value found in this experiment.

The composition of plagioclase changed very little from Run 2K-12 (3 h, 1190°C) to Run 2K-24 (24 h, 1188°C) for two bulk compositions. For composition N50 the plagioclase compositions were, respectively, An 41·9 and 42·3—identical within analytical error. For composition 78 PCS, the results were An 48·2 and 50·7—a moderate change. From this evidence, it appears that plagioclase nucleated and continued to grow near its equilibrium composition, as it cannot have re-equilibrated internally in such short times (e.g. Morse, 1984; Brady, 1995).

By contrast, the composition of olivine in the same two runs changed appreciably with time. In composition N50 at 3 h, the derived K_D value for Fe/Mg was 0·537, whereas, after 24 h, it was 0·321—a typical equilibrium value. For Run 2K-17 (2·8 h, 1220°C) in composition R50a, K_D was 0·418, and in Run 2K-21 (9·1 h, 1217°C) for composition R50aCOT, K_D was 0·349. The evidence suggests that olivine nucleates easily and off-composition during the run-up, and then requires time for diffusive equilibration, which would easily be accomplished in these grain sizes, temperatures and times of 9–24 h (Brady, 1995).

Table 5: Glass analyses for critical runs defining the cotectic

Ser. No.	Run	Composition:	SiO_2	TiO_2	Al_2O_3	FeO	MnO	MgO	CaO	Na_2O	K_2O	P_2O_5	Total
		100AvSTD:	41	4	14	21	3	8	9	9	2	5	
		STD ±	14	2	7	8	1	5	3	8	1	2	
1	KI 1·1	KI BC96pl	50·44	0·67	19·59	11·08	0·11	5·77	8·33	3·44	0·28	0·08	99·79
2	2K 47·3	KI BC3pl	48·91	0·69	18·74	13·50	0·16	6·97	7·96	3·69	0·23	0·13	100·98
3	2K 47·2	KI BC2pl	49·32	0·73	18·89	13·11	0·14	6·86	8·08	3·74	0·24	0·11	101·22
4	KI 20·1	KI BC3ol	48·47	0·69	18·12	13·52	0·15	6·73	7·91	3·67	0·23	0·10	99·59
5	KI 45·3	KI BC3cot	48·93	0·91	17·30	14·72	0·22	5·94	7·54	3·80	0·27	0·09	99·72
6	2K 17·1	R50agl	47·67	0·87	16·58	16·61	0·25	6·19	7·62	3·64	0·18	0·10	99·71
7	2K 21·123	R50acot	47·64	0·93	16·69	16·89	0·24	5·70	7·81	3·63	0·20	0·15	99·88
8	2K 40·1	R65acot	47·14	1·01	16·16	16·62	0·28	5·56	8·09	3·82	0·33	0·21	99·22
9	2K 17·2	R65agl	48·03	0·95	15·75	16·47	0·24	5·67	7·72	3·74	0·30	0·19	99·06
10	KI 53·1	new50P	49·69	0·97	15·76	14·36	0·26	5·64	8·42	3·70	0·32	0·34	99·46
11	2K 44·2	R75acot	47·41	0·99	14·69	16·72	0·28	5·25	9·35	3·69	0·26	0·45	99·09
12	2K 44·3	78 PCScot	48·48	0·97	14·39	15·39	0·29	5·34	9·49	3·89	0·32	0·55	99·11
13	2K 12·2	78 OL	49·81	0·85	13·79	16·84	0·30	4·97	8·93	3·63	0·29	0·42	99·83
14	KI 42·1	KI BC4bcot	50·07	0·70	15·94	12·43	0·20	6·59	10·36	3·00	0·24	0·09	99·62
15	2K 45·2	UZ4cot	49·70	0·37	14·36	15·02	0·27	4·64	10·06	3·83	0·32	0·04	98·61
16	2K 45·1	UZ3cot	49·93	0·39	14·28	14·87	0·26	4·53	10·05	3·84	0·32	0·02	98·49
17	KI 37·1	KI UZ3plaug	50·98	0·43	14·46	15·14	0·25	4·43	9·71	3·49	0·33	0·06	99·28
18	KI 36·1	KI UZ2aug	51·20	0·40	14·11	15·69	0·25	4·51	9·68	3·58	0·30	0·05	99·77

All analyses 10 points on glass except No. 7, 2K21, 15 points. The second row of the table gives the average standard deviation for each oxide, multiplied by 100, and the third row ('STD ±') gives the standard error of that average.

Crystal settling and compositional convection

Crystal distribution within the sample charges was examined in two samples that were cut and polished along the length of the charge. These were samples KI 56-1 (KI50PCS, 1215°C: Pl + *L*) and KI 56-2 (New50PCS, 1205°C: Pl + Ol + *L*). Both runs show apparent evidence of crystal settling. In KI 56-1 (8 h), plagioclase crystals appear 400 μm below the top of the charge and increase in both size and abundance over the next 800 μm to the bottom of the charge. Run KI 56-2 (2 h) shows similar behavior; plagioclase appears 200 μm below the top of the charge and olivine appears 600 μm below the top. Both plagioclase and olivine increase in size and abundance over the length of the charge. In some runs, the crystallization at depth of unseen olivine was revealed simply by the low Mg-ratio found at the top of the charge.

Several possible interpretations, none mutually exclusive, may explain these observations. There may have been physical crystal settling, especially of olivine. There may well have been compositional convection of dense rejected solute from plagioclase that caused the nucleation of olivine at depth in the charge. There may also have been thermal migration in a temperature gradient (Lesher & Walker, 1988).

RESULTS: COTECTIC EQUILIBRIA

Critical runs

Experiments with scarce crystals in glass that constrain the cotectic trace include bracketing or nearby equilibria *L*(Ol) and *L*(Pl), as well as cotectic *L*(Ol,Pl) equilibria. The equilibrium *L*(Aug) constrains the end of the Lower Zone cotectic trace. Eighteen such constraining runs are here called critical to the interpretation of the liquid line of descent. Glass analyses of these runs are presented in Table 5, arranged in reverse PCS order and listed by serial number. Working run numbers from Electronic Appendix 1 are given in column 2. The third column gives the bulk composition with an appendage that indicates whether the partly crystallized glass was in equilibrium with plagioclase, olivine, both of these ('cot'), or augite. One glass without crystals (No. 9) is included because it is close in composition to its cotectic partner, No. 8. The oxygen norms of these glass analyses are given in Table 6. The serial numbers correlate inversely with

Table 6: Oxygen norms of analyses in Table 5

SerNo	AP	MT	IL	OR	AB	AN	DI	HY	OL	NE,LC	SUM	X_{An}	X_{Mg}	X^{o}_{Mg}	FSP	AUG	OLHY	OLRAT
1	0·18	1·10	0·91	1·72	31·55	38·43	2·8	15·49	7·82		100·00	0·549	0·541	0·5088	0·733	0·034	0·233	0·871
2	0·29	1·34	0·92	1·15	34·57	35·04	3·67	2·48	20·53		99·99	0·503	0·535	0·5073	0·726	0·045	0·229	0·835
3	0·25	1·29	0·97	2·72	34·38	35·06	4·08	2·47	19·77		100·99	0·505	0·541	0·5119	0·730	0·050	0·220	0·814
4	0·26	1·36	0·93	1·17	34·51	34·10	4·61	3·84	19·23		100·01	0·497	0·527	0·4985	0·716	0·057	0·227	0·800
5	0·18	1·47	1·26	1·76	35·78	30·98	5·94	5·17	17·45		99·99	0·464	0·478	0·4461	0·706	0·073	0·221	0·750
6	0·26	1·68	1·22	1·19	35·00	30·14	6·90	1·67	21·95		100·01	0·463	0·453	0·4258	0·685	0·085	0·230	0·729
7	0·30	1·73	1·28	1·19	35·03	30·46	7·35	1·67	21·00		100·01	0·465	0·432	0·4028	0·690	0·091	0·219	0·706
8	0·45	1·70	1·40	2·40	32·96	27·68	10·56	0·00	20·75	2·10	100·00	0·449	0·429	0·3994	0·672	0·111	0·218	0·663
9	0·45	1·69	1·34	1·79	35·83	27·28	9·41	3·02	19·18		99·99	0·432	0·436	0·4069	0·672	0·117	0·211	0·643
10	0·74	1·47	1·32	1·76	35·28	26·94	11·03	9·04	12·42		100·00	0·433	0·468	0·4365	0·663	0·137	0·200	0·593
11	1·02	1·71	1·41	1·21	33·16	24·42	16·96	0·00	18·31	1·81	100·01	0·419	0·412	0·3830	0·628	0·179	0·193	0·519
12	1·20	1·59	1·34	1·79	35·87	22·42	18·16	0·00	16·74	0·90	100·01	0·382	0·439	0·4085	0·634	0·190	0·175	0·480
13	0·93	1·73	1·17	1·78	35·05	21·80	16·93	9·02	11·58		99·99	0·383	0·396	0·3690	0·610	0·211	0·179	0·459
14	0·18	1·26	0·98	1·75	28·00	30·74	17·06	10·61	9·41		99·99	0·523	0·543	0·5124	0·620	0·210	0·170	0·448
15	0·07	1·55	0·51	1·80	35·33	22·64	23·13	0·00	14·07	0·90	100·00	0·388	0·399	0·3791	0·618	0·237	0·144	0·378
16	0·08	1·55	0·56	1·20	36·60	22·50	23·18	0·00	13·73	0·60	100·00	0·380	0·395	0·3754	0·621	0·238	0·141	0·372
17	0·11	1·53	0·61	2·37	33·16	24·17	19·99	10·66	7·40		100·00	0·422	0·388	0·3675	0·611	0·245	0·144	0·370
18	0·11	1·57	0·55	1·77	34·24	22·84	21·03	9·41	8·48		100·00	0·400	0·383	0·3633	0·602	0·258	0·140	0·352

OLRAT is OLHY/(OLHY + AUG). X is mole fraction. X^{o}_{Mg} is mole fraction Mg/(Mg + Fe) before magnetite is formed in the oxygen norm of the glass.

Table 7: Summary of critical runs for the cotectic

Ser. No.	OLRAT	Comp	Run	FRACTION FELDSPAR IF xl IS:					*T*,°C	*t*, h	Products
			FIELD:	PL	OL	PL + OL	AUG	SP			
1	0·871	KI BC96pl	KI 1·1	0·733					1235	40	gl70 pl30
2	0·835	KI BC3pl	2K47·3	0·726					1240	3	gl98 pl2 oltr
3	0·814	KI BC2pl	2K47·2	0·730					1240	3	gl95,pl5,oltr
4	0·800	KI BC3ol	KI 20·1		0·716				1230*	16·5	gl99,ol1
5	0·750	KI BC3cot	KI 45·3			0·706			1210	6	gl65,pl25,ol10
6	0·729	R50agl	2K17·1		0·685				1220	2·8	gl99,ol1
7	0·706	R50aCot	2K21·123			0·690			1217	9·1	gl97,pl2,ol1
8	0·663	R65aCOT	2K40·1			0·672			1207†	3	gl96pl3ol1
9	0·643	R65agl	2K17·2	0·672					1220	2·8	gl100
10	0·593	New50P	KI 53·1	0·663					1205	2	gl96,pl3,oltr
11	0·519	R75acot	2K44·2			0·628			1203†	3	gl98pl2oltr
12	0·480	78PCScot	2K44·3			0·634			1203	3	gl96pl3ol1
13	0·459	78 OL	2K12·2		0·610				1199†	3	gl97,ol3
14	0·448	KI BC4bCot	KI 42·1			0·620			1210†	8·5	gl79,pl15,ol6
15	0·378	UZ4cot	2K45·2			0·618		SP	1205†	3	gl93pl5aug2
16	0·372	UZ3cot	2K45·1			0·621		SP	1205†	3	gl96pl3ol1
17	0·370	KI UZ3plaug	KI 37·1	0·611					>1180	6	gl94,pl5,aug1
18	0·352	KI UZ2gl	KI 36·1				0·602		>1180	6	gl99,aug1

OLRAT is the ratio OLHY/(OLHY + AUG). SP, augite saturation point; tr, trace.
*At 4·5 kbar. All others at 5 kbar.
†Corrected *T*.
This table is organized according to serial number. The middle five columns each give the ternary feldspar content from column 16 of Table 6, listed by column according to the liquidus phase (Pl, Ol, Cotectic Pl+Ol, Aug, or four-phase saturation point, SP). These separations of the data allow each series to be plotted with its own distinctive symbol.

the ratio OLRAT given in the last column, which is the measure of the relative proportions of olivine plus hypersthene to olivine plus hypersthene plus augite; hence, the serial numbers correlate directly with the augite content of the glasses. The run products, conditions and normative glass compositions for the critical runs for the cotectic are summarized in Table 7.

The cotectic trace

The cotectic trace was determined from the experimental data of Table 7, plotted in Fig. 8. The regression has the relation $Y = 0{\cdot}252X + 0{\cdot}512$, $r^2 = 0{\cdot}96$, as shown in the figure. The standard error of Y is 0·01, or 1% feldspar. The high correlation coefficient and low standard error are taken to justify accepting the cotectic trace as linear in this XY space. The cross symbol near point 4 is the Inner Border Zone average from Table 1.

At its high-temperature end, the cotectic trace is fixed at AUG = 5·2% (Fig. 2). This augite content occurs at a calculated ratio OLRAT = 0·817 at 0 PCS (Fig. 8). At the low-temperature end, the cotectic trace is terminated at the experimentally determined point of saturation with augite (Fig. 8). Four near-liquidus glass compositions listed in Table 7 constrain the location of the saturation point involving all three solid phases. Glass 17 (Fig. 8), with plagioclase on the liquidus, constrains the Pl–Aug boundary to lie below that glass composition and above glass 18. Glass 18 has augite on the liquidus, so the Aug–Ol boundary lies to the right of that point (a square in Fig. 8). The two glass compositions 15 and 16, run in the same assembly, straddle the augite field boundary, as follows. Both runs contain 3–5% plagioclase and 93–96% glass. In addition, glass 16 contains 1% olivine, and glass 15 contains 2% augite. It is interesting to note the direction in which these cotectic compositions came from their glass parents (Fig. 3): to the right and down from bulk composition UZ4 to glass 15, and up from bulk composition UZ3 to glass 16. The observed mafic phases are each on the 'wrong' side of the Aug–Ol field boundary with respect to each other, according to the glass analyses, but they are the same within analytical error.

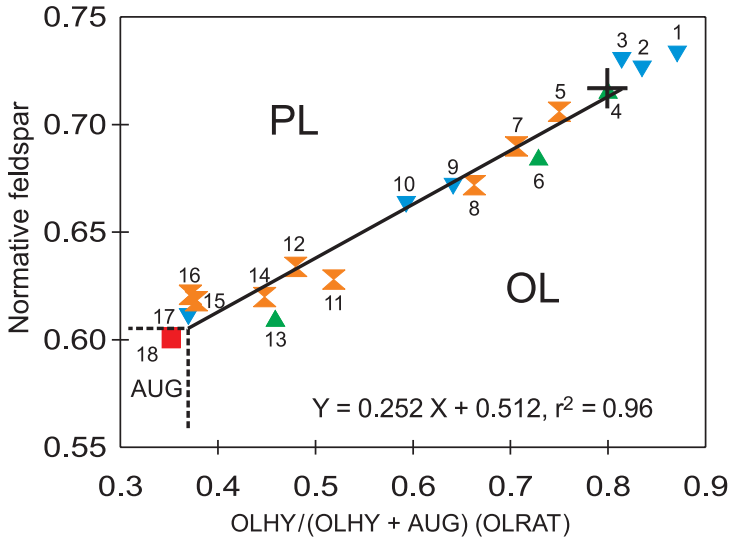

Fig. 8. Plot of the critical run data from Table 7. Inverted blue triangles: liquidus *L*(Pl); upright green triangles, liquidus *L*(Ol); orange double triangles, cotectic *L*(Pl,Ol); red square, liquidus *L*(Aug). Note that the refractory sample BC4bcot (point 14) is consistent with other cotectic symbols having less refractory values of AN and FO. The cross symbol near point 4 represents the Inner Border Zone average from Table 1. Points 1–3 were included in the regression (continuous line) but they have less augite component than the 5·2% considered as the starting point of the Lower Zone liquid path. Points 15–18 constrain the augite saturation point, as discussed in the text. Normative Ne in samples 8, 11, 12, 15 and 16 was converted to Ab for the purposes of this plot.

The OLRAT values of the two glass compositions 15 and 16 are 0·378 and 0·372, respectively (Table 7), for an average of 0·375; therefore, the augite saturation point is estimated to lie at OLRAT 0·375 ± 0·003 and FSP = 61%.

DISCUSSION OF THE COTECTIC TRACE

Effects of AN, FO, excluded elements and pressure on the cotectic

We wished to test the sensitivity of the cotectic trace to variations in several compositional and extensive properties of the experiments. Variations in neighboring compositions, or in groups of compositions, can be used to test whether the location of the cotectic trace might be systematically affected, within the composition range encountered.

Combined AN, FO variation

The composition KI BC4bcot (point 14) was designed to be rich in augite component without change in plagioclase or olivine composition. It therefore differs from compositions that contain less refractory plagioclase and olivine components. After 21% crystallization, the original plagioclase-rich bulk composition (Fig. 3) has moved to the cotectic point 14, on the cotectic trace within uncertainty. Nearby glasses 12, 13, 14 have normative AN 38, 38 and 52 (Table 7), and (as X^{o}_{Mg}) FO 44, 40 and 54, respectively. Within this range of variation, there is no effect of AN and FO, *taken together*, on the position of the cotectic in terms of its feldspar content.

Minor elements

The high phosphorus values listed in Table 5 belong to the compositions 8–13. Of these, all but composition 13 lie at or near the cotectic (Fig. 8). The low-phosphorus compositions are 1–7 and 14–18. As with AN and FO, the triplet 12, 13, 14 suggests that a 5- or 6-fold variation in P content has no effect on the location of the cotectic. Similar arguments can be made for the excluded elements Ti and K. For Ti, nine runs with high values, averaging 0·94% TiO_2 in points 5–14, plot consistently with four runs having low values, averaging 0·40% TiO_2 in points 15–18 of Fig. 8. The high values are 2·4 times the low values, without systematic, detectable effect on the cotectic position. For the run glasses in Table 5, the K/Na ratio averages 0·075 ± 0·003 ($S/\sqrt{N}$, $N = 18$), whereas, in the LZ rocks (Morse, 1981*b*), the ratio averages 0·064 ± 0·002 ($N = 14$). The glasses have significantly higher K/Na than the rocks, as appropriate for liquids compared with rocks. Variations in Ti, K and P do not appear to have any systematic effect on the feldspar content of the cotectic.

Pressure

Studies in progress (Banks *et al.*, 2002) on compositions KI BC2 and KI BC3 also show that there is almost no

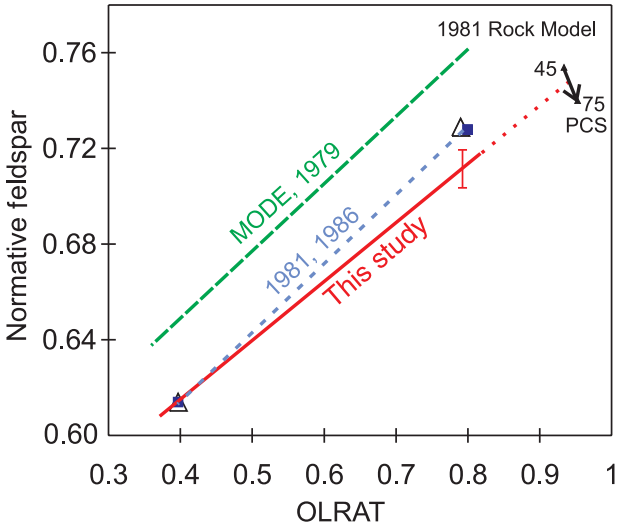

Fig. 9. Comparison of the Lower Zone liquid paths estimated from summation over the rock density and modal data (Morse, 1979*a*, 1979*b*), as transformed to the chemistry (Morse, 1981*b*; Nolan & Morse, 1986), and as obtained experimentally in this study. The modal data are in volume percent; all other data are referred to the oxygen norm; the ~3% feldspar separation of the modes and norms is characteristic, as seen in Table 1. The regressions on the modal and summation paths have correlation coefficients $r^2 = 0{\cdot}997$–$0{\cdot}999$ for the Lower Zone. End-points for the 1981*b* liquid path are shown as open triangles; those using the corrected ferric iron content in the 1986 study are shown as small squares; the results are indistinguishable. The rock models from 45 to 75 PCS (Morse, 1981*b*) span the backward extension of the experimental cotectic trace, consistent with an average Lower Zone rock near 55 PCS acting as the fractionating rock composition operating on the cotectic liquid path.

change in the cotectic position for these compositions at pressures up to 15 kbar. In sum, only AUG has a discernible effect on the FSP content of the *L*(Pl,Ol) cotectic. This result was already predicted from the closely parallel location of the modal liquid path compared with the cotectic in Fo–Di–An (Osborn & Tait, 1952) shown in fig. 23 of Morse (1979*b*), where it was estimated that the effect of Ab in Pl is compensated by Fa in Ol, with little pressure effect.

Comparison of experimental and calculated cotectics

The experimental cotectic trace from Fig. 8 is compared to the modal track (Morse, 1979*b*) and the chemical estimates (Morse, 1981*b*; Nolan & Morse, 1986) in Fig. 9. The high-temperature intercepts for the modal and chemical estimates are the same, at an *X*-axis value of 0·80, whereas the starting point was set back to a value of 0·817 (5·2% augite) in this study. The low-temperature intercepts for the modal and chemical study are set at the calculated equilibrium saturation point with augite (Morse, 1979*b*), at an *X*-axis value of 0·36 for the mode and 0·40 for the chemical estimate at 81 PCS. The augite saturation point determined in this study falls at $X = 0{\cdot}38$, as discussed above, halfway between the earlier two estimates. All four estimates agree within reasonable uncertainty. The experimental study therefore tends to confirm the earlier calculations in terms of the long excursion to saturation with augite. Note that the inferred pressure of crystallization of the Kiglapait Intrusion is 2·5 kbar, compared with the experiments made at 5 kbar, so there is apparently little, if any, pressure effect on the location of the cotectic trace in this pressure range, as found also by Banks *et al.* (2002).

Average Lower Zone rocks tend to become slightly more olivine-rich at higher stratigraphic levels (Morse, 1979*b*, 1981*b*), as indicated by the 'Rock Model' arrow from 45 to 75 PCS in Fig. 9. By itself, this feature would justify some concave-up curvature of the cotectic trace to make the rock path lie on a sweep of tangents to the liquid path. No such attempt is made here, although the data shown in Fig. 8 might permit it, but at least it can be said that some average Lower Zone rock near 55 PCS certainly may lie on the extension of the cotectic trace, as determined in this study.

The feldspar content at the high-temperature end of the experimental cotectic trace is lower (by <2% feldspar) than expected from the chemical estimate from Morse (1981*b*) and Nolan & Morse (1986). Although the difference is small, it could mean that the exposed, early-formed Lower Zone rocks are slightly plagioclase-rich relative to the *L*(Pl,Ol) equilibrium.

Ternary representation

The *XY* plot of FSP versus OLRAT, used in Figs 1, 3, 8 and 9, may be transformed to the ternary coordinates FSP, OLHY, AUG (Table 1) by the following relations, FSP being already defined as an apex:

$$\mathrm{OLHY} = \mathrm{OLRAT} \times (1 - \mathrm{FSP})$$

$$\mathrm{AUG} = 1 - (\mathrm{OLHY} + \mathrm{FSP}).$$

The straight 1 atm *L*(Ol,Pl) cotectic in Fo–Di–An (Osborn & Tait, 1952) was modified by Morse (1979*b*) to extend metastably through the spinel field to the peritectic point *L*(Fo,An,Sp) in the join Fo–An, as found in fig. 3 of Osborn & Tait (1952). The cotectic must curve concave toward An to meet this constraint. A linear array or regression in the *XY* composition plot is a curve that is concave toward the FSP apex in the ternary, as is the case for the modal path derived from rock densities (Morse, 1979*a*, 1979*b*). Therefore, a rigorously linear treatment of the data in *XY* space is consistent with the curvature required in the ternary. The *XY* plot was chosen in this study because it crosses altitudes in FSP with radial lines OLRAT most nearly at right angles (exactly so at OLRAT = 0·50).

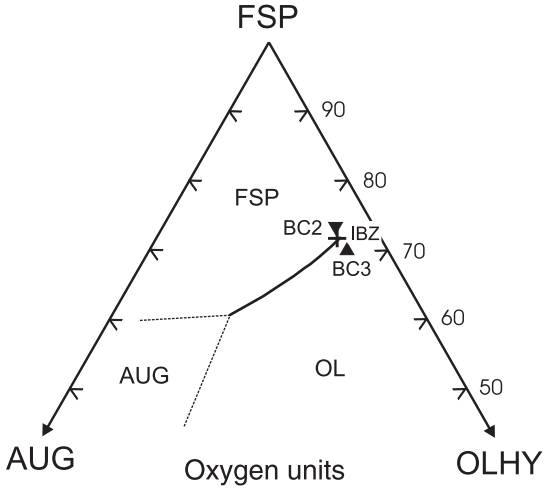

Fig. 10. Ternary expression of the LLD, with bracketing bulk compositions KI BC2pl (Table 5, number 3) and KI BC3 (Table 4) for comparison; they are labeled BC2 and BC3. Also shown is the IBZ average from Fig. 8. The straight line in the *XY* plot (Fig. 8) is concave toward FSP in the ternary, as also found in the pure end-member system Fo–Di–An and in the modal data (Morse, 1979*b*).

The experimental ternary cotectic trace of the Lower Zone LLD, transformed from the *XY* plot (Fig. 8) is shown in Fig. 10, where the saturation point with augite is indicated by the schematic field boundaries of the augite field. Point BC3 is the bulk composition glass, whereas point BC2 is glass plus 5% plagioclase (Table 7) with a trace of olivine (there is not enough olivine to interpret the run as truly cotectic). The IBZ average (cross) is very close to the upper terminus of the cotectic trace.

Length of the cotectic trace

The length of the ternary cotectic track furnishes an opportunity to estimate the degree of crystallization for the Lower Zone by applying the Lever Rule. This estimate may be considered justified by the fact that 97% of the composition estimates in Table 1 lie in the ternary plane. An ideal Lower Zone adcumulate rock would plot on the OL–FSP sideline. However, the actual LZ rocks contain small amounts of augite that crystallized from trapped liquid. In the norms calculated for the Lower Zone rock models (table 5 of Morse, 1981*b*), the average *di* over the range 15–82·5 PCS is 1·3%. (The oxygen normative AUG has the same value.) From the stipulated initial condition (Fig. 2), we have 5·2% AUG in the bulk composition. The saturation point with augite is given by point 17 (Table 6, Fig. 8) as 24·5% AUG. Taking the partial difference divided by the total difference, (24·5 – 5·2)/(24·5 – 1·3) = 0·83 as the fraction solidified, or 83 PCS. This value is close to the 81 PCS modal estimate for the equilibrium saturation point with augite (Morse, 1979*b*).

The cotectic trace found here clearly shows that troctolitic liquids may generate very large masses of troctolite before they reach saturation with augite (Scoates & Mitchell, 2000). Moreover, this long excursion across the ternary is consistent with the field interpretation that little, if any, recharge of the magma chamber occurred after the deposition of the basal Lower Zone, contrary to the hypothesis of DePaolo (1985).

Compositions sought and found

Because the experimental mineral compositions listed in Electronic Appendix 1 are mainly from runs of short duration, we do not use these for comparison with the natural data. Instead, we made a series of longer runs, summarized in the partitioning section below, in order to derive the linear partitioning relationships that can be used to retrieve the *equilibrium* compositions of crystals *at the liquidus* (or cotectic). Comparisons with the natural data can then be more rigorously made by inverting liquids to crystals, or vice versa, using the partitioning equations.

A test of the glass compositions in terms of AN and FO for the critical runs is shown in Fig. 11. In Fig. 11a are plotted all measured pairs of plagioclase and olivine compositions for the Lower Zone. The glass compositions from Table 7 have been inverted to paired Fo,An values for the crystals, obtained from the equilibrium partitioning values mentioned in the caption. Except for the most refractory glasses 2, 3 and 4, the results are well distributed throughout the field of the natural composition pairs. By contrast, the line of intended compositions [from equations (1) and (2)] falls near the low-Fo edge of the field. The end results are more representative of the natural rocks than the model results.

In Fig. 11b and c, the compositions of plagioclase and olivine are plotted against stratigraphic height, as represented by the PCS (or F_L) scale. Here, the observed crystal compositions are inverted to their equilibrium liquids, shown by the vertical lines. Among these are plotted the normative glass compositions from Table 6, with stratigraphic position based on the normative AUG-content of the liquid [Fig. 2 and equation (5)]. Bearing in mind that the aim of the experimental study was to bypass the natural data from 0 to 30 PCS, so as to extrapolate the Lower Zone trend to a fictive end-point at 0 PCS, the match of inverted liquids to the experimental cotectic melt compositions is very satisfactory.

Comparison with natural examples

The Kiglapait Upper Border Zone (Allison, 1986) has yielded one sample that appears from its bladed texture and fine-grained mafics to be a roof-chilled sample—in effect, a quenched liquid (sample KI 4085, with texture shown in fig. 7 of Morse, 1982). This sample has the

composition SiO_2 48·17, TiO_2 2·15, Al_2O_3 15·05, Fe_2O_3 2·40, FeO 12·24, MnO 0·21, MgO 6·75, CaO 9·28, Na_2O 3·17, K_2O 0·43, P_2O_5 0·31, sum 100·16 (analysis by XRF at UMass). The normative AUG-content is consistent with an equivalent stratigraphic level of 75·5 PCS [Fig. 2a; equation (5)]; hence, a ferrous ratio of 0·84 (Fig. 2b) was assigned in the above analysis. The oxygen norm of this analysis has OLRAT 0·484, FSP 63·6, $An_{47.3}$ and $X^{o}_{Mg} = 0{\cdot}49$. This composition is plotted as a large gray triangle in Fig. 12, where it is seen to fall on the experimental cotectic taken from Fig. 8. However, for comparison with our usual reference base using ferrous ratio 0·9, the position shifts to OLRAT 0·494, FSP 63·3, as shown by the bold triangle. This is a credible sample of an intermediate Kiglapait liquid.

Although no other samples of Kiglapait liquids along the cotectic line of descent are known to exist, they may have analogues in another place. The 1305 ± 5 Ma Newark Island Layered Intrusion (NILI), just south of the Kiglapait Intrusion in Labrador, is a composite body of troctolite and granite cumulates (Wiebe, 1988). Feeder structures contain spectacular, strongly chilled pillows of resident mafic magma, engulfed by granitic magma during replenishment of the chamber. The chilled rinds of these mafic pillows show little contamination from the granite and may be taken as representative of a succession of mafic magmas in the intrusion. Wiebe (1988, fig. 15) projected the compositions of 90 mafic dikes and chilled pillows onto the CMAS system and showed that they clustered closely to the olivine–plagioclase cotectic in that system, and could be reasonable parents of the coarser-grained cumulates. Oxygen normative compositions of chilled pillow analyses 3–8 from table 1 of Wiebe (1988) are plotted as large boxes in Fig. 12 for comparison with the cotectic trace determined in this study. The small boxes in Fig. 12 are the data for the large boxes reduced in feldspar content by 0·025. Although the NILI data are consistently about 2·5% more felsic than our cotectic, they shadow it closely and provide natural examples of liquids of varying augite content resulting from the fractionation of troctolitic parental magmas. Moreover, the textures of the chilled pillows (fig. 8 of Wiebe, 1988) show radiating clusters of plagioclase, implying growth from

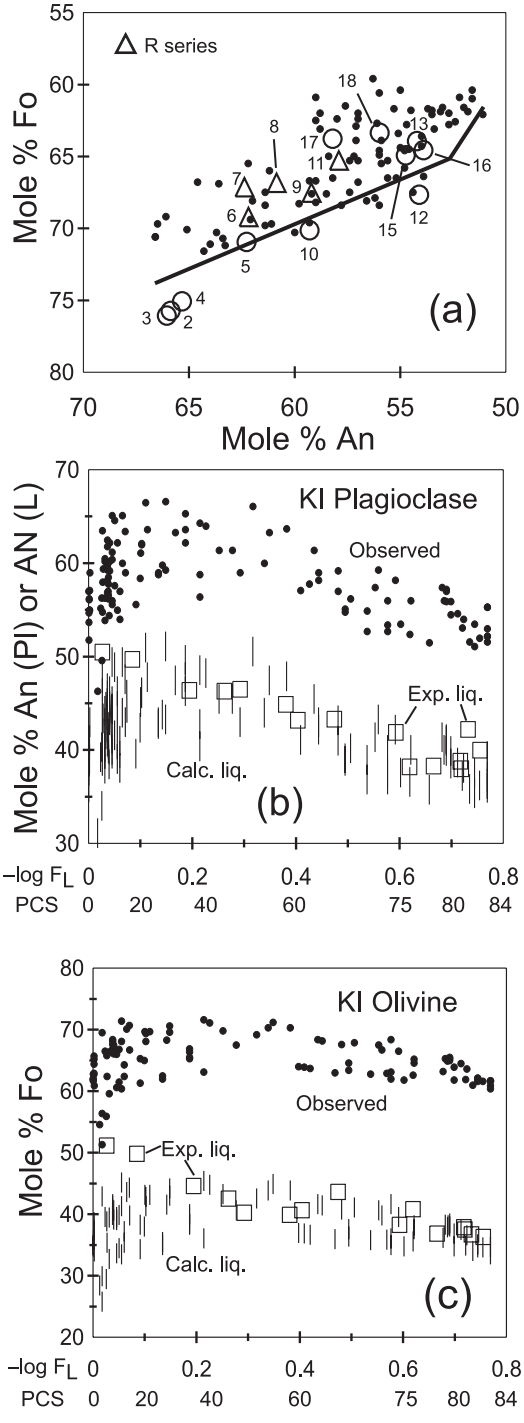

Fig. 11. (a) Plot of 86 pairs of olivine and plagioclase compositions from the Kiglapait Lower Zone to 84 PCS, with cotectic liquid compositions from Table 6 inverted to crystal compositions (circles and triangles) using $K_D = 0{\cdot}33$ for olivine and 0·524 for plagioclase, as found experimentally (see section on partitioning, below). The line is obtained from the composition equations (1) and (2) in the text, with extension from 80 to 84 PCS for olivine from table 2 of Morse (1996). The inversion was done with the linear partitioning relation using equation (5) of Morse (2000). Compositions 1 and 14 in Table 6 were not inverted. (b) Plagioclase compositions plotted against PCS for the Lower Zone. The calculated normative liquids are obtained from the observed crystal compositions via the linear partitioning relation using $K_D = 0{\cdot}524 \pm 0{\cdot}037$. The length of an individual bar is equal to the uncertainty in the calculation, based on the uncertainty in K_D. Boxes represent the norms of experimental cotectic liquids from Table 6, omitting Nos 1, 2 and 14. The experimental liquids satisfactorily represent the target compositions. Model compositions below 30 PCS are extrapolated from higher stratigraphic levels in order to represent the least crystallized parent magma. (c) Observed olivine compositions, with calculated and experimental liquid compositions as for (b), using $K_D = 0{\cdot}33$.

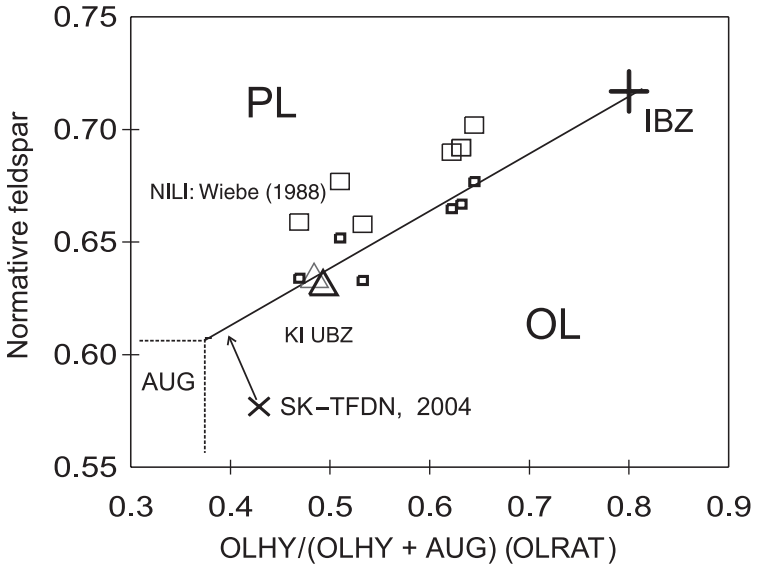

Fig. 12. Compositions of three natural occurrences compared to the cotectic trace of Fig. 8. The composition of a chilled rock, KI 4085, from the Kiglapait Upper Border Zone (KI UBZ), calculated at a ferrous ratio of 0·9, is shown as a large bold triangle, and at a ferrous ratio of 0·84, a gray triangle. Shown as large open squares are the compositions of six troctolitic chilled pillows from the Newark Island Layered Intrusion south of the Kiglapait Intrusion ('NILI', Wiebe, 1988) that were quenched against an engulfing granitic magma. These chilled margins show a trend of evolution toward increasing augite content. The small squares are the same data after subtracting 2·5% normative feldspar. The estimated bulk composition of the Skaergaard Intrusion ('SK-TFDN', Nielsen, 2004) would imply considerable fractionation of olivine (trajectory shown by the arrow) before reaching the *L*(Pl,Ol) condition that is seen in the Skaergaard Lower Zone. However, the fractionation of olivine would lead to an appropriately small interval of troctolite crystallization before the liquid became saturated with augite (Wager & Brown, 1968).

plagioclase-supersaturated melts, so the Newark Island feldspar content may well be metastably enhanced.

The Skaergaard Intrusion shows a small Lower Zone of cumulus plagioclase and olivine, succeeded by augite as a cumulus phase (Wager & Brown, 1968). A new estimate of the bulk composition of that intrusion (Nielsen, 2004) is plotted in Fig. 12, for comparison with the cotectic trace and augite field determined here. Nielsen's estimate lies well within the olivine field, significantly off the cotectic condition inferred from the field evidence. A significant amount of olivine fractionation would be expected from such a composition. However, the trajectory of olivine fractionation does lead to a very small cotectic (Ol + Pl) Lower Zone before saturation with augite, as seen in the field.

TEMPERATURE ANALYSIS

Extrapolated liquidus (i.e. limiting cotectic) temperatures were assigned along the liquid line of descent, using compositions lying at or near the cotectic. These values were obtained from visual estimates of glass percentage, extrapolated with calibrated plots of percent glass versus temperature (typically 2·7% glass/deg), to find the fictive temperature at 100% glass. The results (±5°C) are shown in Fig. 13. When plotted against OLRAT, Fig. 13a, the data show a steep initial slope from about 1245°C at the beginning of crystallization (OLRAT ~0·8) declining to a shallower slope and reaching augite saturation at 1204°C. A similar temperature variation is seen in the plot against normative AN (Fig. 13b).

The solidus of an artificial cumulate, KI 4845ac, was found to lie between the entirely crystalline condition in Run KI 16-3 at 1235°C, 5 kbar, 7·5 h, and the partly melted condition in Run KI 17-3 at 1240°C, 5 kbar, 17 h (temperatures corrected +5°C from Sporleder, 1998). This result is taken as the nominal upper bound of the liquidus at 21 PCS, the average stratigraphic level of the olivine and plagioclase that make up the artificial cumulate, as described in the section on bulk compositions. The apparent solidus temperature of 1237·5°C is plotted as a triangle at the coordinates of the 21 PCS stratigraphic level in Fig. 13. The plotted points are consistent with the liquidus determinations, emphasizing the value of the solidus determination as a maximum estimate of the crystallization temperature.

The actual emplacement pressure of the Kiglapait Intrusion was probably near 2·5 kbar (Berg, 1977, 1979, 1980), rather than 5 kbar, as in our experiments. Using a Clapeyron slope of ~8°C/kbar, the emplacement temperature would have been 1245°C – 20 = 1225°C. The temperature interval for the entire Lower Zone now drops from the previously estimated 85°C (Morse, 1979*a*, 1980) to the experimental 42°C, emphasizing the very shallow cotectic slope for troctolitic liquids. A very similar emplacement temperature of 1230°C was

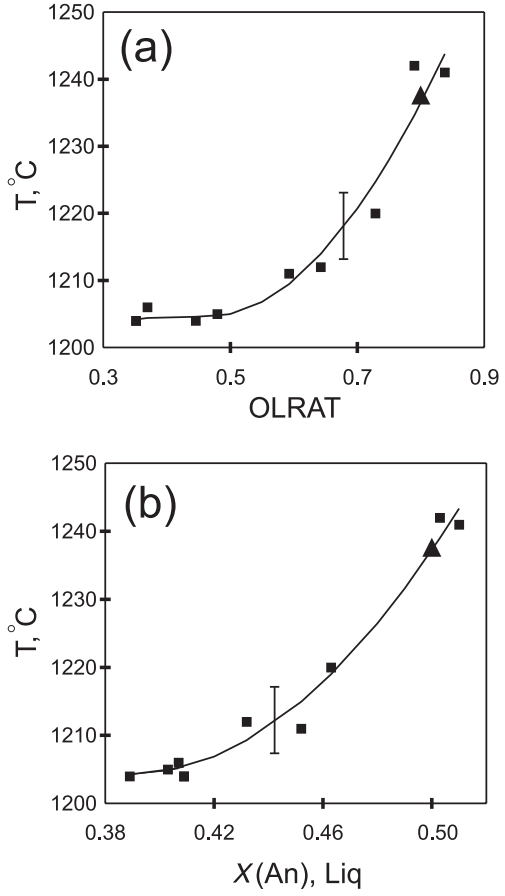

Fig. 13. Experimental cotectic temperatures for the Kiglapait Lower Zone, determined by extrapolation to 100% glass from partly crystallized runs. (a) Temperatures plotted against OLRAT. (b) The same results plotted against the plagioclase composition in the glass (Liq). The triangle is the solidus of the artificial cumulate KI 4845 described in the text, plotted at its nominal stratigraphic position at 21 PCS. The triangles were not used in the regressions, but, instead, support them independently. The curves are polynomial fits to the data, representing an exponential decrease in temperature.

calculated by Barmina & Ariskin (2002) for a pressure of 2·2 kbar.

PHASE EQUILIBRIA MODELING USING MELTS

MELTS is a Gibbs free energy minimization algorithm, developed by Ghiorso & Sack (e.g. 1995) for modeling chemical mass transfer in magmatic systems. Toplis & Carroll (1995) have shown that care must be taken when applying MELTS to ferro-basaltic systems, owing to a scarcity of relevant information within the experimental database. A tendency for the program to over-stabilize pyroxene was discussed by Gaetani (1998). In order to assess its relevance to Al–Fe-rich systems, MELTS was tested against our experimental results.

Fractional crystallization paths were calculated for bulk compositions KI BC2 and KI BC3, using the experimental conditions $P = 5$ and 2·5 kbar and $fO_2 = FMQ - 2$. This fO_2 was used to reflect, if anything, a more reducing environment than is estimated for these graphite-capsule piston-cylinder conditions. MELTS finds (in April 2004) the liquidus temperatures for KI BC2 10°C high, and for KI BC3 31°C high, compared with our values of 1241 and 1242°C. The predicted liquidus phases do not agree with our experimental results. Our experiments at 5 kbar show plagioclase on the liquidus of KI BC2 and olivine on the liquidus of KI BC3 (Figs 5 and 10), whereas MELTS predicts clinopyroxene and orthopyroxene, respectively. In MELTS, composition KI BC2 shows Cpx at 1251°C, followed by Pl at 1245°C, and no other phase to 1200°C. Composition KI BC3 shows Opx at 1273°C, followed by Cpx at 1248°C and Pl at 1242°C, to 1200°C. No olivine appears in either bulk composition over the temperature intervals examined: 51–73°C. Predicted phase equilibria agree somewhat better at lower pressures. At 2·5 kbar, KI BC3 shows Ol at 1223°C, Pl at 1220°C and Cpx at 1200°C, so at least the crystallization sequence is appropriate. These results suggest that the discrepancies arise from a paucity of high-pressure data in the MELTS database. The present data could help to remedy this deficiency.

BULK COMPOSITION OF THE EXPOSED INTRUSION

The bulk compositions BC2 and BC3 straddle the cotectic at the inferred beginning of crystallization, so their average makes a good reference point for the bulk composition of the intrusion. This average yields the observed crystal compositions of olivine and plagioclase. It is shown in column 2 of Table 8, where it is compared with the summation composition of the intrusion (Morse, 1981*b*) given in column 1, and the average composition of the Inner Border Zone, both from Table 1. The average Inner Border Zone composition (Figs 8 and 10) is very close to the high-temperature end of our experimental cotectic trace in terms of feldspar content, OLRAT value and plagioclase composition, but not olivine composition (Table 8; $Fo_{61.9}$).

The bulk compositions BC2 and BC3 in this work are deficient in Ti and K (Table 8, column 2), so it is reasonable to retain the values for those elements from the summation composition, as given in column 3. The highlighted oxides and normative quantities in Table 8 show the principal differences between the summation and the experimental results. The IBZ composition is similar to column 3 in the excluded elements Ti, K and P. Column 3 of Table 8 may be considered a best estimate of the Kiglapait magma composition as presently exposed,

Table 8: Experimental bulk composition compared to other estimates

Oxide	1	2	3	4	Norms	1	3	4
SiO_2	49·27	48·96	48·55	48·07	AP	0·25	0·25	0·26
TiO_2	0·79	0·63	0·79	0·76	MT	0·96	1·31	1·65
Al_2O_3	18·72	18·58	18·43	18·46	IL	1·08	1·09	1·04
FeO_T	**10·25**	13·24	**13·13**	**11·76**	OR	1·73	1·74	1·75
MnO	0·15	0·15	0·15	0·16	AB	28·78	33·72	32·10
MgO	**7·80**	7·06	**7·00**	**7·94**	AN	37·41	34·77	35·78
CaO	**9·55**	8·03	**7·96**	8·21	DI	7·99	4·14	4·38
Na_2O	**3·09**	3·64	**3·60**	3·44	HY	6·69	3·27	3·50
K_2O	0·27	0·22	0·27	0·29	OL	15·11	19·69	19·55
P_2O_5	0·11	0·11	0·11	0·12	An/PL	**56·5**	**50·8**	**52·7**
Total	100·00	100·62	100·00	99·20	X^o_{Mg}	**0·598**	**0·516**	**0·619**
					FSP	69·5	72·2	71·7
					AUG	9·8	5·1	5·4
					OLHY	20·7	22·7	22·8
					OLRAT	0·678	0·817	0·809

1, KI 1981 summation, Table 1. 2, Average of KI BC2 and KI BC3 glasses. 3, Same, but with Ti and K from KI 1981. 4, IBZ average from Table 1.

consistent with the An and Fo values of the cumulate rocks produced, and co-saturated with olivine and plagioclase at a low concentration of augite.

OLIVINE–PLAGIOCLASE–MELT RELATIONS

Olivine–plagioclase intergrowths

In run 2K21·1, held at 1217°C, sample R50a fell exactly on the cotectic, and formed a spectacular eutectoid intergrowth of plagioclase and olivine (Fig. 14). The plagioclase evidently grew 10 times faster than the normal experimental growth rate (at ~10 cm/yr rather than the usual ~1 cm/yr), and, in so doing, captured olivine in excess of the commonly observed 74/26 Pl/Ol cotectic ratio. Analogous intergrowths were found in 1 atm runs by Blundy (1997, fig. 1). In Fig. 14, streamers of mafic rejected solute (RS) are seen flowing away from the plagioclase surfaces. Olivine appears to have nucleated periodically from these RS streamers. The plagioclase–olivine intergrowths appear to be topotactic, controlled by the plagioclase structure, but, in fact, the control is remote from the plagioclase crystal surface, as seen in the bottom row of olivine crystals outside the plagioclase. The outer edges of the olivine crystals are sub-parallel to the plagioclase surfaces, but they evidently only lie along the concentration front outboard of the plagioclase crystal. The streamers of rejected solute have the

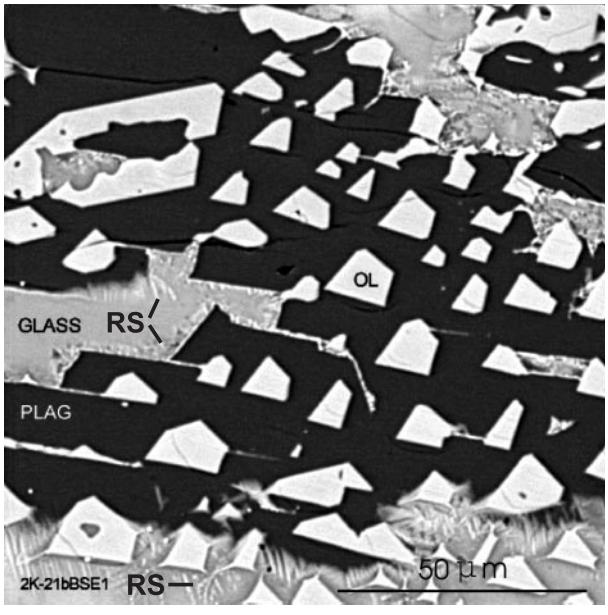

Fig. 14. BSE image of a plagioclase–olivine eutectoid intergrowth from bulk composition R50a, held exactly on the cotectic at 1217°C for 9·1 h, run 2K-21. Sparse nuclei of plagioclase grew at 10 times the normal growth rate in our runs, i.e. ~10 cm/yr instead of ~1 cm/yr, and, in so doing, captured olivine in excess of the expected 74:26 cotectic ratio. Note the streamers of mafic rejected solute (RS) from the plagioclase and the periodic nucleation of olivine therefrom. Also note the partial and complete melt inclusions in Ol. The Plag–Ol interface appears to be controlled mainly by the PL structure, but, in fact, the control is remote, apparently dictated by a concentration front, as seen in the bottom row of Ol crystals outside the plagioclase.

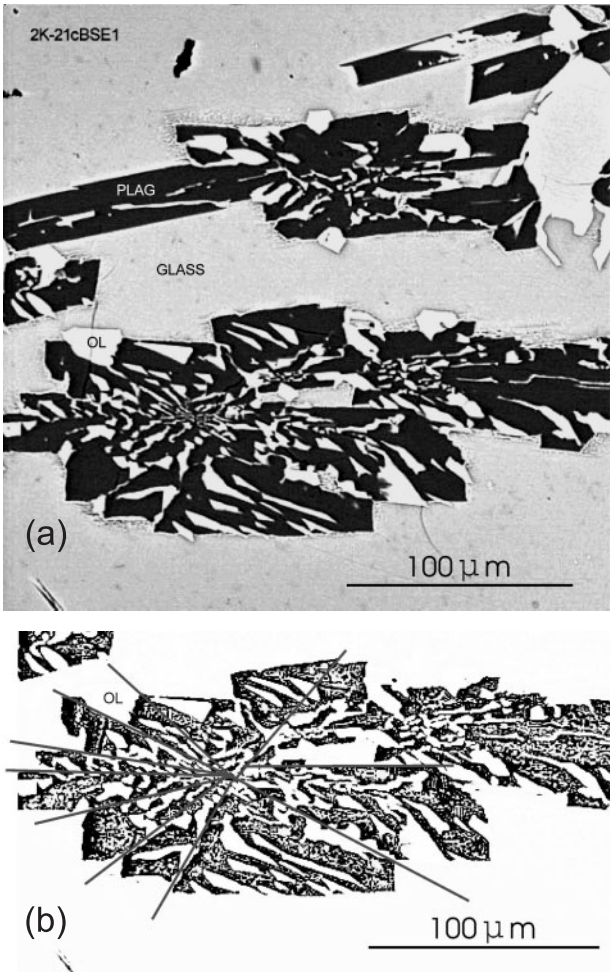

Fig. 15. BSE images of a large Pl–Ol snowflake with 10 blades of plagioclase and lots of occluded olivine, run 2K-21. (a) General view showing surroundings and another snowflake. (b) High-contrast image of Fig. 15a, with radial lines showing the grain boundaries.

potential to drive compositional convection (Morse, 1969: 71) and may, in fact, represent the early stages of compositional convection in action.

Elsewhere in the section, the plagioclase crystals form a radiating microspherulite with 10 individual blades in the plane of section (Fig. 15). Here, again, the olivine content of the intergrowth appears to exceed significantly the expected equilibrium cotectic ratio. The individual plagioclase crystals are shown by the radiating lines from a common central area in Fig. 15b.

Discussion

In the snowflake troctolites of the nearby Hettasch and Vernon Intrusions (Berg, 1980; Berg *et al.*, 1994), the nucleation and growth of olivine from supercooled mafic liquid drove the residual liquid into the plagioclase field, where it formed plagioclase spherulites up to 15 cm in diameter and more. In the Hettasch case, a melatroctolite magma flowed into the existing troctolitic chamber and crystallized abundant sugary dunite, which then drove the liquid into the plagioclase field, where plagioclase nucleated in suspended macrospherulites. In this experimental case, the rare nucleation of plagioclase from scarce centers has driven the interstitial boundary liquid metastably into the olivine field and caused it to nucleate in over-abundance. The pathways to the natural and experimental textures are different. However, the causes of the radial structure are similar; they are a result of supersaturation, sparse nucleation and rapid growth. If the natural occurrence grew at the laboratory rate, the Hettasch snowflakes would have grown in a year.

Subsolidus olivine–plagioclase reaction

The depleted Ca content of plutonic olivines relative to volcanic and experimental samples has long been recognized, and identified, as a problem in thermodynamic calculations such as QUILF (Andersen *et al.*, 1993; Davidson & Lindsley, 1994). The case for the Kiglapait olivines was discussed by Morse (1996), who could find no satisfactory exchange reaction between olivine and plagioclase to account for the loss of Ca in the olivine of troctolites. A serendipitous diffusion-reaction experiment in the present study helps to resolve the problem of Ca gain and loss in olivine, by confirming plagioclase as a source of Ca on heating and, hence, by inference, a sink for Ca on cooling.

Electron microprobe analysis of olivine grains in the subsolidus artificial cumulate KI 4845ac in run KI 16·3, held at 1235°C, 5 kbar for 7·5 h, revealed Ca-rich rims on Ca-poor cores. Ca imaging revealed that the rims were ubiquitous on olivine against plagioclase. The core compositions averaged $Fo_{73\pm1}$ and contained CaO = 0·0705 ± 0·016 wt % (n = 4)—a normal abundance for the natural Ca-depleted olivines in the Kiglapait Intrusion (Morse, 1996). Rim compositions measured on two grains were $Fo_{75\pm1}$ and contained CaO = 0·238 ± 0·034 wt %. This >3-fold increase in Ca in only 7·5 h, to 6·7 cations permil, is well on the way to the apparent equilibrium value of 10 cations permil, earlier found in a run of 23 days at 1225°C, 5 kbar in a South Margin sample (Morse, 1996, fig. 3). The result confirms that olivine can steal Ca from plagioclase very rapidly at high temperature. The small change in Fo content may signify that an exchange of Ca for Fe could occur in this reaction. If the olivine can gain Ca from plagioclase so readily at high temperature, then it can surely lose it to plagioclase over geologic time while cooling to a blocking temperature at a rate of ~50°C/Myr (Yu & Morse, 1992), so the mechanism for the loss of Ca in plutonic olivines is now becoming apparent, despite the lack of a precise reaction.

PARTITIONING STUDIES

Major components in plagioclase

The concept of linear partitioning is embodied (but long hidden) in the discovery of a constant K_D near 0·3 for olivine–liquid pairs by Roeder & Emslie (1970). In fact, this constant is the unconstrained, empirical intercept of a linear partitioning relationship for which the other intercept has the value of 1·0 (Appendix B). The case for plagioclase is different from that of olivine, because compositional and pressure effects may generate a wide range of intercept values, quite apart from any experimental problems. It is, therefore, critical for modeling purposes to find the appropriate linear partitioning relationships for plagioclase in the Kiglapait system and related compositions. To this end, feldspar and glass compositions were determined for eight runs, longer than 7·5 h. The analyses are given in Table 9, and the results are summarized in Table 10 and Fig. 16. The three most Ab-rich of these runs are from Peterson (1999). The range of plagioclase compositions is An_{68} to An_{28}—large enough to allow characterization of the partitioning relationship in these compositions at 5 kbar. The array of points in Fig. 16 is unambiguously linear ($r^2 = 0{\cdot}80$) from an *unconstrained* regression intercept value of 1·000, with a K_D value of 0·524 ± 0·037—slightly lower than the value of 0·54 used in making up the bulk compositions for this study. The experimental result (Fig. 16) supports, for the first time, the hypothesis that natural feldspar–liquid pairs are actually linear from the ideal value of 1·0 at $X_{Ab} = 1{\cdot}0$.

Discussion and literature review

The partitioning of crystal–melt pairs in binary solutions is conceptually straightforward in a pure binary system, if both the liquidus and solidus can be located accurately. But, whereas the solidus may be identified with the beginning of melting in the system An–Ab, the crystal composition must be found by equilibration and analysis in a multicomponent system. Equilibration can be difficult to achieve, and there is no consensus about the correct value of $K_D^{(XAb)}$ for plagioclase in dry basaltic liquids. (Here, for the sake of uniformity, we convert various literature data to the same oxygen norm protocol used for liquids in this study.) For example, assuming linear partitioning, 1 atm experiments suggest values of $K_D = 0{\cdot}45$–$0{\cdot}8$ for arc volcanics (Marsh *et al.*, 1990), and $K_D = 0{\cdot}35$–$0{\cdot}5$ for Skaergaard analog liquids (Toplis & Carroll, 1995). A study of MORB equilibria at various pressures to 10 kbar (Grove *et al.*, 1992) shows considerable scatter, but is consistent with a range in K_D of 0·45–0·65, or $K_D = 0{\cdot}02P + 0{\cdot}434$, where P is in kbar. This result gives, incidentally, $K_D = 0{\cdot}534$ at 5 kbar—indistinguishable from our value, above. By contrast, experiments on a possible parent of Harp Lake anorthosite by Fram & Longhi (1992) yield $K_D = 0{\cdot}042P + 0{\cdot}436 \pm 0{\cdot}10$ over the range from 1 atm to 15 kbar. The 1 atm intercept is the same as in the study by Grove *et al.*, but the slope is twice as steep. Referred to 5 kbar, the Fram & Longhi result yields $K_D = 0{\cdot}646$—considerably higher than our value.

The diversity of these experimental results suggests that a multitude of difficulties lies in the way of a comprehensive understanding of plagioclase partitioning. However, the average of the lowest values at 1 atm is 0·42 ± 0·04, which may serve as a consensus value for $K_D^{(XAb)}$ at 1 atm. It is considerably greater than the value of 0·26 found for plagioclase in a melt saturated with Di (Morse, 1997).

The partitioning data from Table 10 and Fig. 16 are most appropriately compared with the experimental piston-cylinder results of Fram & Longhi (1992). Using run durations of 10–141 h, averaging 48 h, these authors studied two bulk compositions: an anorthosite dike from the Nain Plutonic Suite, Labrador, and a chilled margin composition from the Harp Lake anorthositic intrusion, Labrador. They gave plagioclase partitioning data from 1 atm to 27 kbar for the anorthosite dike, and to 15 kbar for the chilled margin. The results are shown in Fig. 17, where $K_D^{(XAb)}$ is plotted against pressure. Each data point from Fram & Longhi represents a single crystal–melt pair, from which $K_D^{(XAb)}$ was calculated assuming linear partitioning. The result from Fig. 16, representing a regression on eight experiments, is shown for comparison by the star symbol.

The anorthosite dike contains ~90% modal plagioclase (87% normative); HLCA contains 65% normative plagioclase in a high-alumina basalt composition. The intercepts at 1 atm approximate to a value of $K_D = 0{\cdot}4$. Clearly, the more mafic array, to which the Kiglapait result belongs, has a steeper slope. The very felsic sample, with a much flatter slope, is, provisionally, a good proxy for pure plagioclase. This diagram contains the beginnings of a comprehensive understanding of plagioclase partitioning, in which the effects of composition are clearly separated from the effects of pressure.

Potassium and Fe in plagioclase

The partitioning of K in plagioclase/liquid varies inversely and systematically with An-content, from 0·18 at An_{68} to >1 at An_{28} (Fig. 18). The higher value reflects the inevitable fact that the liquid is diluted with low-K mafic components when the feldspar composition approaches the ternary minimum in An–Ab–Or, where D_K (FSP/L) = 1·0. The values at the low end of the range are similar to those found for dendritic plagioclase in melt at 1 atm on the Kiglapait South Margin sample KI 3763 (Table 1) by Blundy (1997), and to those found by Vander Auwera *et al.* (2000) at pressures from 1 atm to 27 kbar, in which $r^2 = 0{\cdot}91$. According to that study, there appears to be little, if any, pressure effect on the

Table 9: Partitioning analyses for plagioclase

Run	Composition	*t*, h	% Glass	SiO_2	TiO_2	Al_2O_3	FeO_T	MnO	MgO	CaO	Na_2O	K_2O	P_2O_5	BaO	Total	X_{An}	X_{Ab}	D_{Fe}	D_{XAb}	D_K
KI 1·1	KI BC96 GL	40	70, pl30	50·44	0·67	19·59	11·08	0·11	5·77	8·33	3·44	0·28	0·08	n.d.	99·79	0·549	0·451	0·038	0·714	0·179
	PLAG		0	50·89	0	31·2	0·42	0	0	13·88	3·64	0·05		n.d.	100·08	0·678	0·322			
KI 39·1	KIUZ4 GL	7·5	89, pl10ol1	51·41	0·37	14·16	14·78	0·28	4·51	9·54	3·89	0·32	0·03	n.d.	99·29	0·366	0·634	0·040	0·696	0·344
	PLAG		0	53·83	0	28·9	0·59	0	0	11·62	5·07	0·11		n.d.	100·12	0·559	0·441			
2K 14·1	N50PCS GL	24	40, pl40ol20	49·76	1·50	12·30	17·78	0·31	3·99	8·90	3·67	0·50	0·56	n.d.	99·27	0·324	0·676	0·023	0·852	0·673
	PLAG		0	57·19	0	26·39	0·40			8·89	6·69	0·34		n.d.	99·90	0·424	0·576			
2K 14·2	78P3OL GL	24	71, pl20ol6	49·72	1·06	12·72	17·84	0·29	4·10	8·86	3·68	0·37	0·60	n.d.	99·24	0·343	0·657	0·025	0·743	0·303
	PLAG		0	54·55		27·88	0·45			10·77	5·68	0·11		n.d.	99·44	0·512	0·488			
2K 14·3	78PCS GL	24	62, pl30ol6	49·44	1·11	12·49	18·49	0·32	4·05	8·68	3·77	0·40	0·63	n.d.	99·38	0·320	0·680	0·031	0·725	0·328
	PLAG		0	54·60		27·90	0·58			10·69	5·75	0·13		n.d.	99·64	0·507	0·493			
KU 44·2	KI 4079 GL	24	90, pl10	46·83	2·78	8·53	26·26	0·62	0·95	8·24	3·10	1·35	0·98	0·42	100·06	0·164	0·836	0·028	0·828	0·874
	PLAG		0	60·56	0	24·19	0·73	0	0	6·11	7·58	1·18		0·30	100·65	0·308	0·692			
KU 35·1	KI 4083 GL	24	97, pl3	52·07	0·97	11·02	20·73	0·55	0·47	6·75	3·47	2·21	0·34	0·51	99·09	0·200	0·800	0·038	0·879	0·869
	PLAG		0	60·62	0	23·52	0·78	0	0	5·50	7·20	1·92		0·59	100·13	0·297	0·703			
KU 44·1	KI 3381 GL	24	90, pl10	50·52	1·84	10·43	20·98	0·53	0·58	7·32	3·40	2·35	0·62	0·64	99·21	0·169	0·831	0·029	0·872	1·157
	PLAG		0	61·09	0	23·21	0·61	0	0	4·76	6·93	2·72		1·16	100·48	0·275	0·725			

X is mole fraction; An, Ab in glass are from oxygen norm; *D* is partition coefficient crystal/melt.

Table 10: Summary data for plagioclase partitioning

Run	Composition	*t*, h	% Glass	X_{An}	X_{Ab}	D_{Fe}	D_{XAb}	D_K
KI 1·1	KI BC96	40	70, pl30	0·549	0·451	0·038	0·714	0·179
	PLAG			0·678	0·322			
KI 39·1	KI UZ4	7·5	89pl10ol1	0·366	0·634	0·040	0·696	0·344
	PLAG			0·559	0·441			
2K 14·1	N50PCS	24	40pl40ol20	0·324	0·676	0·023	0·852	0·673
	PLAG			0·424	0·576			
2K 14·2	78P3OL	24	71pl20ol6	0·343	0·657	0·025	0·743	0·303
	PLAG			0·512	0·488			
2K 14·3	78PCS	24	62pl30ol6	0·320	0·680	0·031	0·725	0·328
	PLAG			0·507	0·493			
KU 44·2	KI 4079	24	90, pl10	0·164	0·836	0·028	0·828	0·874
	PLAG			0·308	0·692			
KU 35·1	KI 4083	24	97, pl3	0·200	0·800	0·038	0·879	0·869
	PLAG			0·297	0·703			
KU 44·1	KI 3381	24	90, pl10	0·169	0·831	0·029	0·872	1·157
	PLAG			0·275	0·725			

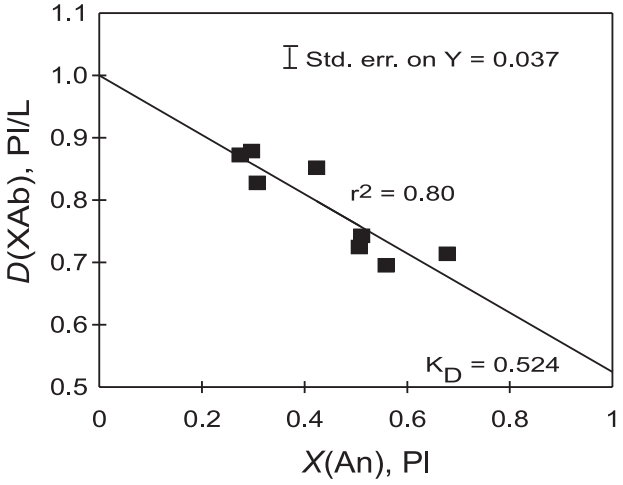

Fig. 16. Linear partitioning of $D(X_{Ab})$ in plagioclase–liquid (Table 9) is demonstrated in these experiments in graphite at 5 kbar, with a best estimate of $K_D = 0{\cdot}524$ (cf. 0·54 estimated earlier and used to make up the bulk compositions). Data from this study and from Peterson (1999). The mole fractions are taken from the cation formulas of the crystals, and from the oxygen norms of the liquids.

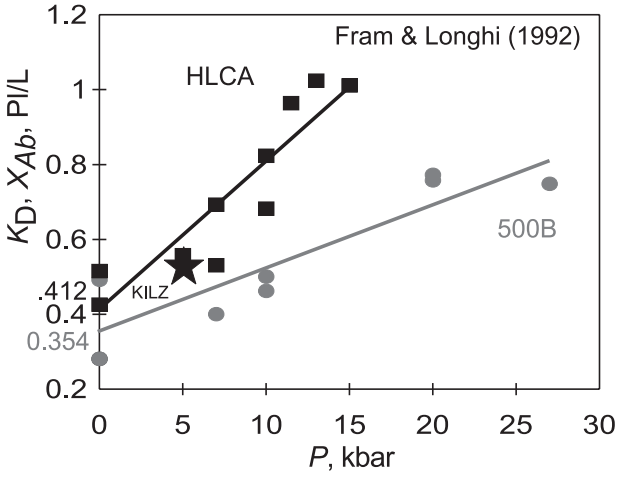

Fig. 17. Plagioclase partitioning at pressure: variation of the intercept constant K_D with pressure as found for two bulk compositions by Fram & Longhi (1992). Composition 500B is an anorthosite dike; composition HLCA is a more mafic composition thought to be parental to the Michikamau anorthosite. Each symbol from the study by Fram & Longhi represents a single experimental result, extrapolated to K_D assuming linear partitioning (Appendix B), as recalculated here with the oxygen norm from the original data. The Kiglapait result (star symbol; KILZ) represents eight experiments (Fig. 16), and, being mafic, belongs to the HLCA group.

partitioning of K in plagioclase. Our values near $D_K = 0{\cdot}2$–$0{\cdot}4$ are well below those predicted from the natural feldspars and calculated liquid compositions of the Kiglapait Intrusion (Morse, 1981*a*), but the trends from the two studies merge near the upper end of the range.

The partitioning of Fe in plagioclase–liquid is very scattered but can be roughly characterized as $D = 0{\cdot}032 \pm 0{\cdot}006$. More runs of long duration are needed to address this imprecise conclusion.

Olivine

Eight runs of 8·5–24 h long were selected for the study of olivine composition relations. The glass and crystal analyses are given in Table 11, and the summary data in Table 12. The results for K_D (Fe–Mg) and D_{Ca} are shown in Fig. 19. The mean value of K_D found was 0·33—the

Table 11: Partitioning analyses for olivine

Run	Comp.	% GI	SiO_2	TiO_2	Al_2O_3	FeO_T	MnO	MgO	CaO	Na_2O	K_2O	P_2O_5	Total	Femol OL	Mgmol OL	Fe/Mg OL	X^{o}_{Mg} GL	Fe/Mg GL	K_D	Fo	D_{Ca}
KI 20·1	KI BC3	99	48·47	0·69	18·12	13·52	0·15	6·73	7·91	3·67	0·23	0·10	99·59								
	OL		37·53	0·00	0·11	23·94	0·25	38·06	0·28	0·00	0·00	0·00	100·17	0·3332	0·9444	0·3528	0·4985	1·0060	0·3507	73·92	0·0354
KI 20·2	KI BC3+pl	99	47·19	0·74	18·68	13·27	0·13	7·55	8·06	3·70	0·22	0·07	99·61								
	OL		37·65	0·00	0·42	23·60	0·24	38·14	0·37	0·00	0·00	0·00	100·42	0·3285	0·9464	0·3471	0·5324	0·8783	0·3952	74·24	0·0459
KI 42·1	KI BC4bCT	79	50·07	0·70	15·94	12·43	0·20	6·59	10·36	3·00	0·24	0·09	99·62								
	OL	Note: KI 42·1 OL data Fo only, complete analysis missing.														0·3550	0·5124	0·9516	0·3731	73·8	n.d.
KI 14·1	KI BC2	77	48·74	0·69	17·91	13·39	0·16	6·70	7·73	3·76	0·25	0·09	99·42								
	OL	Note: KI 14·1 dubious OL data: XFo or FoMn? Ca data in rough notes.															0·5	1·0000	n.d.		0·0349
2K21all	R50aCT	97	47·64	0·93	16·69	16·89	0·24	5·70	7·81	3·63	0·20	0·15	99·88								
	OL		37·13	0·05	0·11	30·58	0·37	33·09	0·28				101·62	0·4257	0·8212	0·5183	0·4028	1·4826	0·3496	65·86	0·0359
2K 14·1	N50P	40	49·76	1·50	12·30	17·78	0·31	3·99	8·90	3·67	0·50	0·56	99·27								
	OL		35·58	0·00	0·01	34·12	0·42	29·33	0·42				99·88	0·4749	0·7278	0·6525	0·3086	2·2404	0·2912	60·51	0·0472
2K 14·2	78XOL	71	49·72	1·06	12·72	17·84	0·29	4·10	8·86	3·68	0·37	0·60	99·24								
	OL		36·12		0·05	33·55	0·40	30·36	0·41				100·89	0·4669	0·7533	0·6198	0·314	2·1847	0·2837	61·74	0·0463
2K 14·3	78PCS	62	49·44	1·11	12·49	18·49	0·32	4·05	8·68	3·77	0·40	0·63	99·38								
	OL		36·06		0·04	34·05	0·47	29·81	0·44				100·87	0·4739	0·7397	0·6407	0·3015	2·3167	0·2765	60·95	0·0507
																		AVG	0·331		0·0423
																		STDEV	0·044		0·0062

Femol and Mgmol are molar proportions of Fe and Mg, respectively. X^{o}_{Mg} is mole fraction Mg/(Mg + Fe) before magnetite is formed in the oxygen norm of the glass. $Fe/Mg = (1/X_{Mg}) - 1$ and $X_{Mg} = 1/(1 + Fe/Mg)$. K_D is [Fe/Mg(crystal)]/[Fe/Mg(melt)]; D_{Ca} is Ca(crystal)/Ca(melt).

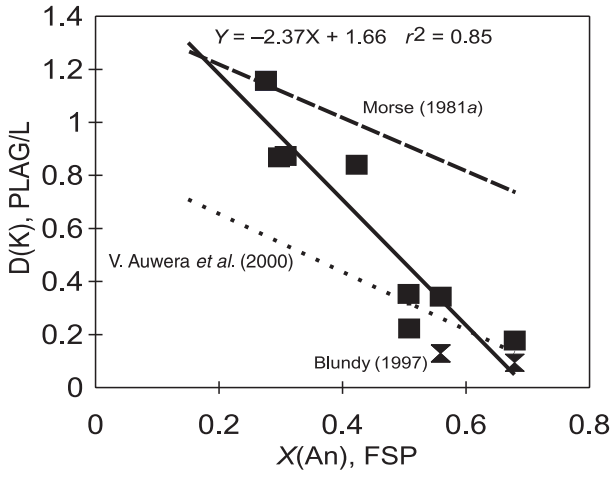

Fig. 18. Partitioning of potassium (K) in plagioclase. The dashed line refers to the summation estimate of Morse (1981*a*) and the dotted line to the experimental study of Vander Auwera *et al.* (2000) at pressures up to 24 kbar. The hourglass symbols refer to the 1 atm experimental study of Blundy (1997). The regression refers to our new data.

Table 12: Summary data for olivine partitioning

Run	Compos.	*t*, h	Fo	K_D Fe—Mg	DCa
KI 20·1	KI BC3	16·5	73·9	0·351	0·0334
KI 20·2	KI BC3+pl	16·5	74·2	0·395	0·0459
KI 42·1	KI BC4bCT	8·5	73·8	0·373	n.d.
KI 14·1	KI BC2	24	69·3	n.d.	0·0349
2K 21all	R50aCT	9·1	65·9	0·350	0·0365
2K 14·1	N50P	24	58·2	0·291	0·0472
2K 14·2	78XOL	24	60·8	0·284	0·0463
2K 14·3	78PCS	24	59·3	0·277	0·0507
			AVG	0·331	0·0421
			STD	0·044	0·0064

same as the value used in making up the run compositions and in the earlier study of olivine (Morse, 1996). The data suggest a trend of K_D with composition from 0·28 at Fo_{61} to 0·38 at Fo_{74} (Fig. 19a). No trend with run length is demonstrable. The positive slope of the trend is surprising in view of the negative trend usually found (e.g. Toplis & Carroll, 1995; Hoover & Irvine, 1978) and used in the calculations for iron-rich olivine in Morse (1996).

The mean value of D_{Ca} (Ol/L) is 0·042 (Fig. 19b), and the values and a negative trend with Fo are similar to those found by Toplis & Carroll (1995).

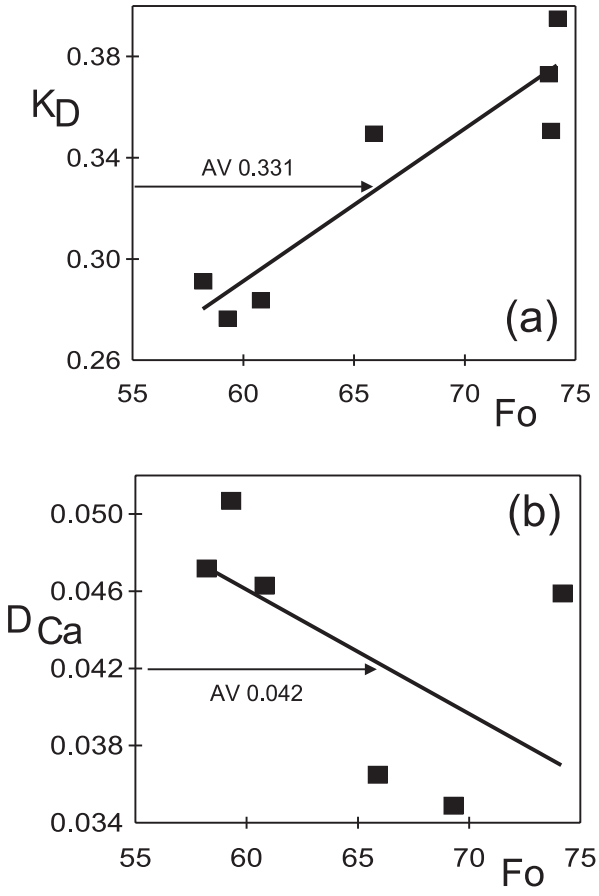

Fig. 19. (a) Exchange coefficient K_D (Fe–Mg) for olivine in experimental runs, plotted against the olivine crystal composition (mole % Fo). (b) Partition coefficient for Ca in olivine–liquid.

REMAINING PROBLEMS

Potassium disparity

The low values of D_K for the range $An_{40–60}$ (Fig. 18) are at odds with the high K contents of the natural feldspars and the summation over all the LZ rocks (Morse, 1981*a*). Similarly, the implied values of D_K in many other plutonic and volcanic systems are far too low to account for the slow evolution of these systems, as shown in Morse (1981*a*). High values of K in the LZ liquids, consistent with the low values of *D* found experimentally, would yield rapid evolution toward K-feldspar not seen until the upper-level rocks of the Upper Zone are reached. The *effective* partition coefficient for K must, then, have been closer to 1·0 than the equilibrium values determined here. Processes that render effective partition coefficients different from equilibrium ones are reviewed in detail by O'Hara & Herzberg (2002). One process known to have occurred in the Kiglapait Intrusion was the capture of K in the Upper Border Zone, where it resides chiefly in red oxybiotite. However, it is not likely that this transfer would quantitatively satisfy the apparent deficit in potassium.

Liquid evolution: evidence from NILI

A disparity exists between the equilibrium liquid compositions found here for FO and AN in the Lower Zone,

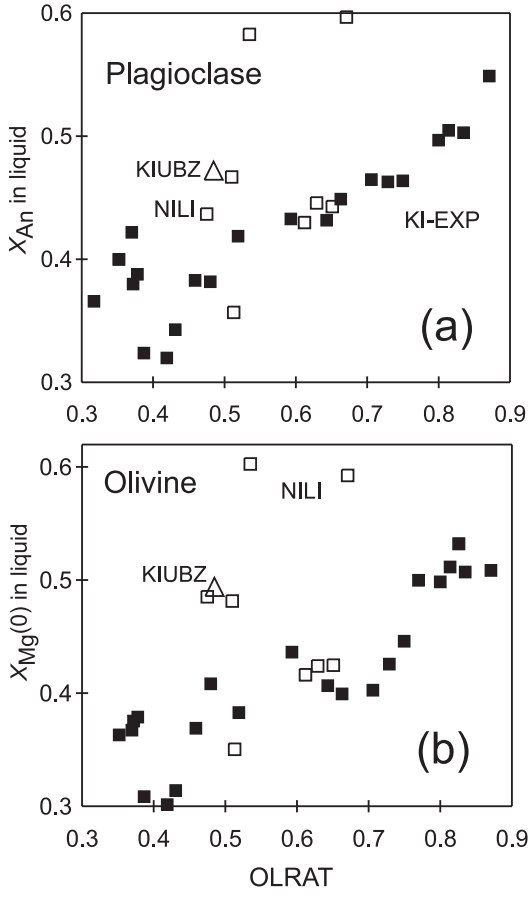

Fig. 20. Plagioclase (a) and olivine (b) compositions in troctolitic dikes and chills of the nearby Newark Island Layered Intrusion (NILI; Wiebe, 1988: table 1), shown as open squares, compared with the experimental glasses from this study (solid symbols). Point 14 of Table 6 and the Upper Zone data in Table 10 are omitted. The NILI data include two dikes and six chills. In (a), one dike and one chill are clearly refractory outliers, but the rest of the points arguably lie within the experimental population. In (b), the case is more dubious, but at least four NILI points lie within the experimental population. The UBZ sample KI 4085 has mineral compositions that are more refractory than the experimental model, but similar to some of the NILI data.

and the summation liquids of Morse (1981*b*), as discussed in Morse (1996). Previous comparisons of these two trends have been defective in several ways, both in the assignment of the equilibrium liquid (which should be based on augite compositions in the Upper Zone) and in the derivation of the summation liquid (with allowance for Al in augite, ordinarily assigned to anorthite in the norm, for example). These matters are under review for a future report. However, we do have external evidence bearing on the variation of FO and AN values, with fractionation progress defined by the augite content of the liquid, as represented by OLRAT.

In Fig. 12, it was shown that chilled pillows from the Newark Island Layered Intrusion (NILI; Wiebe, 1988) may share the same cotectic trend as the experimental data from this study. Here, we enquire whether the normative plagioclase and olivine compositions of these chills and their associated dikes in table 1 of Wiebe (1988) may also plot among the experimental data for the liquid compositions in terms of AN and FO. Figure 20 shows the results of this comparison.

For the plagioclase composition (Fig. 20a), there is a definite trend of positive correlation, to which all but one NILI dike and one chill may reasonably be considered to belong. The UBZ sample KI 4085 is shown as a triangle for comparison. The olivine composition (Fig. 20b) is more equivocal, but at least four of the NILI points clearly belong to the same population as the experimental data. As with the plagioclase plot, the UBZ sample is high relative to the experimental trend, but within the NILI group.

Several explanations for the similar evolution of liquids in the two intrusions come to mind. The first proposition is that the two sets of liquids are actually one and the same, and that NILI represents periodic squirts from the Kiglapait magma chamber into the Newark chamber. This would involve transit of liquid pulses about 15 km to the south. There is no field evidence, nor any other evidence, to suggest such a transfer, but neither criterion can be called definitive. The second proposition is that two similar parental magmas evolved independently at different places and times. Given the widespread regional presence of at least eight mapped troctolitic intrusions (Ryan, 1990), the second proposition seems the more likely. Assuming that to be the case, then, the results shown in Fig. 20 (and in Fig. 12) would suggest the parallel evolution of two magma bodies, of very different sizes, along the same fractionation path. The NILI data have the advantage of being concrete natural examples of an evolving troctolitic liquid. They suggest that simultaneous progress toward augite enrichment and depletion in refractory mineral compositions occurred according to a common process in which the operative, or effective, partitioning between feldspar and liquid, and olivine and liquid, was the same as in the Kiglapait intrusion.

If this tentative conclusion is correct, then the natural evolution of mineral compositions in troctolitic magma is best modeled by multiphase Rayleigh fractionation, as used in Morse (1996), to model the evolution of olivine composition. This procedure recovers the evolution of the liquid as recorded in the crystal compositions.

CONCLUSIONS

Natural starting materials from the Kiglapait intrusion serve well in mixing bulk compositions and growing large crystals relevant to locating the cotectic trace for the Lower Zone. The experimental melts reach saturation

with augite at the same value of OLRAT as predicted from the modal data at ~81 PCS. A comparable estimate of fractionation progress is obtained by use of the Lever Rule on the ternary cotectic. This result is consistent with the multiphase Rayleigh fractionation of olivine of a composition calculated to match the observed olivine variation in the Kiglapait Intrusion. Experimental liquidus temperatures for the Lower Zone liquid line of descent (LLD) correlate as expected with the augite content of the experimental melts, and with An in plagioclase.

The experimental results permit a revised estimate of the bulk composition of the exposed rocks of the Kiglapait intrusion, richer in the low-temperature components of plagioclase and mafic minerals than an earlier result by summation over the exposed rocks. This work appears to constitute the first experimental determination of an LLD for a layered intrusion at pressure. It shows that troctolitic liquids exist in the laboratory and that the average Inner Border Zone composition lies nearly on the *L*(Ol,Pl) cotectic near the high-temperature end of the LLD, despite having a more refractory olivine composition than the appropriate LZ liquid.

Rapid crystallization of both plagioclase and olivine from a cotectic melt has produced mosaic textures and compositional streamers that yield insights into competitive crystal growth from Fe-rich silicate melts. Radial intergrowths of plagioclase and olivine in the laboratory resulted from fast crystal growth at the olivine–plagioclase cotectic, simulating, in principle, the origin of snowflake troctolites in nature. A sintered artificial cumulate of olivine and plagioclase shows strong Ca enrichment of the olivine rims in 7·5 h, leading to a better understanding of the depletion of Ca in slowly cooled plutonic olivines. A test of the postulated exchange reaction of Ca for Fe is a fertile target for future research.

Partitioning studies in longer runs show that D_{XAb} in plagioclase–melt pairs follows a linear partitioning relation with $K_D = 0{\cdot}524 \pm 0{\cdot}037$ at 5 kbar. This relationship allows the calculation of X_{An} in equilibrium liquid compositions and permits the forward calculation of liquid evolution by fractional crystallization, as in the classical case of olivine.

The determination of parent liquid compositions for plutonic igneous rocks is famously an inverse problem, and the present exercise is no exception. Finding experimental melts that yield the crystal compositions observed in the field does not guarantee that such melts, per se, actually produced the rocks seen. But, the melts found do constitute members of a class that could have given rise to the observed rocks, and, by careful study of the variables attending the use of these natural compositions, we may conclude that the results found here probably have an important bearing on the origin and evolution of the Kiglapait magma. They also have tangible counterparts in the Upper Border Zone and in the nearby Newark Island intrusion.

ACKNOWLEDGEMENTS

Troels Nielsen kindly furnished a preprint of his useful Skaergaard paper. We thank Bruce Watson and Bernie Wood for helpful suggestions. The clarity of presentation has benefited from the efforts of Neil Irvine in many strenuous and mostly dissenting reviews, and from critical reviews by Don Lindsley, Richard Naslund, Gregor Markl, Bill Meurer and Jon Blundy. Mike Jercinovic was helpful in overseeing the electron microprobe analyses and back-scattered electron imaging. This research was supported in part by the Earth Sciences Division, NSF grant EAR-9526262 and amendments.

SUPPLEMENTARY DATA

Supplementary data for this paper are available from the *Journal of Petrology* online.

REFERENCES

Allison, J. P. (1984). Petrography of the Upper Border Zone of the Kiglapait intrusion, Labrador. MS thesis, University of Massachusetts.

Andersen, D. J., Lindsley, D. H. & Davidson, P. M. (1993). QUILF: A Pascal program to assess equilibria among Fe–Mg–Mn–Ti oxides, pyroxenes, olivines, and quartz. *Computers & Geosciences* **9**, 1333–1350.

Banks, D. C., Morse, S. A. & Brady, J. B. (2002). OL–PLAGIOCLASE reaction to Al–CPX + OPX + SP + LIQ at 13 kb and the partitioning of PL/L. *EOS Transactions, American Geophysical Union* **83**, S365–S366.

Barmina, G. S. & Ariskin, A. A. (2002). Estimation of chemical and phase compositions for the initial magma of the Kiglapait troctolite intrusion, Labrador, Canada. *Geochemistry International* **40**, 972–983.

Berg, J. H. (1971). The petrology of the outer and inner border zones of the Kiglapait layered intrusion. MS thesis, Franklin and Marshall College.

Berg, J. H. (1974). Further study of the Hettasch intrusion and associated rocks. In: Morse, S. A. (ed.) *The Nain Anorthosite Project, Labrador: Field Report 1973. University of Massachusetts Department of Geosciences Contribution* **13**, 107–119.

Berg, J. H. (1977). Dry granulite mineral assemblages in the contact aureole of the Nain Complex, Labrador. *Contributions to Mineralogy and Petrology* **64**, 32–52.

Berg, J. H. (1979). Physical constraints and tectonic setting of the Nain Complex. *Geological Association Canada—Mineralogical Association Canada Program with Abstracts* **4**, 39.

Berg, J. H. (1980). Snowflake troctolite in the Hettasch intrusion: evidence for magma mixing and supercooling in a plutonic environment. *Contributions to Mineralogy and Petrology* **72**, 339–351.

Berg, J. H. & Docka, J. A. (1983). Geothermometry in the Kiglapait aureole, Labrador. *American Journal of Science* **283**, 414–434.

Berg, J. H., Emslie, R. F., Hamilton, M. A., Morse, S. A., Ryan, A. B. & Wiebe, R. A. (1994). Anorthositic, granitoid, and related rocks of the Nain Plutonic Suite. *International Geological Correlation Programme, IGCP Projects* #290 and #315, 69 pp.

Blundy, J. D. (1997). Experimental study of a Kiglapait marginal rock and implications for trace element partitioning in layered intrusions. *Chemical Geology* **141**, 73–92.

Brady, J. B. (1995). Diffusion data for silicate minerals, glasses, and liquids. In: Ahrens, T. J. (ed.) *Mineral Physics and Crystallography: A Handbook of Physical Constants*. *American Geophysical Union Reference Shelf* **2**, 269–290.

Davidson, P. M. & Lindsley, D. H. (1994). Effect of Ca content and SiO_2 activity on augite + olivine equilibria. *American Mineralogist* **79**, 1123–1124.

DePaolo, D. J. (1985). Isotopic studies of processes in mafic magma chambers: I. The Kiglapait Intrusion, Labrador. *Journal of Petrology* **26**, 925–951.

Fram, M. S. & Longhi, J. (1992). Phase equilibria of dikes associated with Proterozoic anorthosite complexes. *American Mineralogist* **77**, 605–616.

Gaetani, G. A. (1998). Igneous petrology. *Science* **282**, 1834–1835.

Ghiorso, M. S. & Sack, R. O. (1995). Chemical mass transfer in magmatic processes IV. A revised and internally consistent thermodynamic model for the interpolation and extrapolation of liquid–solid equilibria in magmatic systems at elevated temperatures and pressures. *Contributions to Mineralogy and Petrology* **119**, 197–212.

Grove, T. L., Kinzler, R. J. & Bryan, W. B. (1992). Fractionation of Mid-Ocean Ridge basalt: In: Morgan, J. P., Blackman, D. K. & Sinton, J. M. (eds) *Mantle Flow and Melt Generation at Mid-Ocean Ridges*. *American Geophysical Union Monograph* **71**, 281–310.

Hoover, J. D. & Irvine, T. N. (1978). Liquidus relations and Mg–Fe partitioning on part of the system Mg_2SiO_4–Fe_2SiO_4–$CaMgSi_2O_6$–$CaFeSi_2O_6$–$KAlSi_3O_8$–SiO_2. *Carnegie Institution of Washington Yearbook* **77**, 774–784.

Huntington, H. D. (1979). Kiglapait mineralogy I: apatite, biotite, and volatiles. *Journal of Petrology* **20**, 625–652.

Kalamarides, R. I. (1984). Kiglapait geochemistry VI: Oxygen isotopes. *Geochimica et Cosmochimica Acta* **48**, 1827–1836.

Kalamarides, R. I. (1986). Oxygen isotope fractionation in the Kiglapait intrusion. *Chemical Geology* **58**, 303–310.

Lesher, C. E. & Walker, D. (1988). Cumulate maturation and melt migration in a temperature gradient. *Journal of Geophysical Research* **93**, 10295–10311.

Marsh, B. D., Fournelle, J., Myers, J. D. & Chou, I.-M. (1990). On plagioclase thermometry in island arc rocks: Experiments and theory. In: Spencer, R. J. & Chou, I.-M. (eds) *Geochemical Society Special Publication* **2**, 65–83.

McBirney, A. R. (1989). The Skaergaard Layered Series: I. Structure and average compositions. *Journal of Petrology* **30**, 363–397.

Morse, S. A. (1969). *The Kiglapait Layered Intrusion, Labrador*. *Geological Society of America Memoir* **112**, 204 pp.

Morse, S. A. (1979*a*). Kiglapait geochemistry I: Systematics, sampling, and density. *Journal of Petrology* **20**, 555–590.

Morse, S. A. (1979*b*). Kiglapait geochemistry II: Petrography. *Journal of Petrology* **20**, 591–624.

Morse, S. A. (1980). Kiglapait mineralogy II: Fe–Ti oxide minerals and the activities of oxygen and silica. *Journal of Petrology* **21**, 685–719.

Morse, S. A. (1981*a*). Kiglapait geochemistry III: Potassium and rubidium. *Geochimica et Cosmochimica Acta* **45**, 163–180.

Morse, S. A. (1981*b*). Kiglapait geochemistry IV: The major elements. *Geochimica et Cosmochimica Acta* **45**, 461–479.

Morse, S. A. (1982). Adcumulus growth of anorthosite at the base of the lunar crust. *Journal of Geophysical Research* **87**, A10–A18.

Morse, S. A. (1984). Cation diffusion in plagioclase feldspar. *Science* **225**, 504–505.

Morse, S. A. (1989). Evidence for thermal migration at an intrusive margin, Kiglapait Intrusion, Labrador. *Terra Abstracts* **1**, 172.

Morse, S. A. (1990). The differentiation of the Skaergaard Intrusion: A discussion of Hunter and Sparks. *Contributions to Mineralogy and Petrology* **104**, 240–244.

Morse, S. A. (1994). *Basalts and Phase Diagrams*. Corrected from 1980 edition and reprinted by Krieger, Melbourne, FL, 493 pp.

Morse, S. A. (1996). Kiglapait mineralogy III: Olivine compositions and Rayleigh fractionation models. *Journal of Petrology* **37**, 1037–1061.

Morse, S. A. (1997). Binary solutions and the lever rule revisited. *Journal of Geology* **105**, 471–482.

Morse, S. A. (2000). Linear partitioning in binary solutions. *Geochimica et Cosmochimica Acta* **64**, 2309–2319.

Morse, S. A. & Allison, J. P. (1986). Correlation between roof and floor cumulates of the Kiglapait intrusion, Labrador. *Geophysical Research Letters* **13**, 1466–1469.

Morse, S. A. & Ross, M. (2004). Kiglapait mineralogy IV: the augite series. *American Mineralogist* **89**, 1380–1395.

Morse, S. A., Lindsley, D. H. & Williams, R. J. (1980). Concerning intensive parameters in the Skaergaard intrusion. *American Journal of Science* **280-A** (Jackson Vol.), 159–170.

Morse, S. A., Rhodes, J. M. & Nolan, K. M. (1991). Redox effect on the partitioning of nickel in olivine. *Geochimica et Cosmochimica Acta* **55**, 2373–2378.

Nielsen, T. F. D. (2004). The shape and volume of the Skaergaard intrusion: implications for mass balances and bulk composition. *Journal of Petrology* **45**, 507–530.

Nolan, K. M. & Morse, S. A. (1986). Marginal rocks resembling the estimated bulk composition of the Kiglapait Intrusion. *Geochimica et Cosmochimica Acta* **50**, 2381–2386.

O'Hara, M. J. & Herzberg, C. (2002). Interpretation of trace element and isotope features of basalts: relevance of field relations, petrology, major element data, phase equilibria, and magma chamber modeling in basalt petrogenesis. *Geochimica et Cosmochimica Acta* **66**, 2167–2192.

Osborn, E. F. & Tait, D. B. (1952). The system diopside–forsterite–anorthite. *American Journal of Science Bowen Vol.*, 413–433.

Peterson, A. L. (1999). Quest for the liquid line of descent of the Upper Zone of the Kiglapait intrusion, Labrador, Canada: an experimental study. MS thesis, University of Massachusetts.

Peterson, A. L., Morse, S. A. & Brady, J. B. (1999). Extreme iron enrichment in graphite-saturated melts of Kiglapait Upper Zone rocks at 5 kb. *EOS Transactions, American Geophysical Union* **80**, F1096.

Prigogine, I. and Defay, R. (1954). *Chemical Thermodynamics*. London: Longmans, Green.

Roeder, P. L. & Emslie, R. F. (1970). Olivine–liquid equilibrium. *Contributions to Mineralogy and Petrology* **29**, 275–289.

Ryan, A. B. (1990). Preliminary geological map of the Nain Plutonic Suite and surrounding rocks (Nain-Nutak, NTS 14 S.W.), scale 1:500 000. St John's, Newfoundland: Geological Branch, Department of Mines and Energy, Map 90-44.

Schuh, M. L. (1981). Geology of the Avakutakh Iron Formation, Labrador. MS thesis, Northern Illinois University, DeKalb, 192 pp.

Scoates, J. S. & Mitchell, J. N. (2000). The evolution of troctolitic and high Al basaltic magmas in Proterozoic anorthosite plutonic suites and implications for the Voisey's Bay massive Ni–Cu sulfide deposit. *Economic Geology* **95**, 677–702.

Speer, J. A. (1978). The stratigraphy and depositional environment of the Aphebian Snyder Group, Labrador. *Canadian Journal of Earth Sciences* **15**, 52–68.

Sporleder, B. A. (1998). Liquid line of descent of the Lower Zone of the Kiglapait layered intrusion, Labrador, Canada: An experimental study. MS thesis, University of Massachusetts.

Stephenson, R. A. & Thomas, M. D. (1978). Three dimensional gravity analysis of the Kiglapait layered intrusion, Labrador. *Canadian Journal of Earth Sciences* **16**, 24–37.

Toplis, M. J. & Carroll, M. R. (1995). An experimental study of the influence of oxygen fugacity on Fe–Ti oxide stability, phase relations, and mineral–melt equilibria in ferro-basaltic systems. *Journal of Petrology* **36**, 1137–1170.

Vander Auwera, J., Longhi, J. & Duchesne, J. C. (2000). The effect of pressure on D_{Sr} (plagioclase/melt) and D_{Cr} (opx/melt): implications for anorthosite petrogenesis. *Earth and Planetary Science Letters* **178**, 303–314.

Wager, L. R. & Brown, G. M. (1968). *Layered Igneous Rocks*. London: Oliver & Boyd.

Watson, E. B., Wark, D. A., Price, J. D. & Van Orman, J. A. (2002). Mapping the thermal structure of solid-media pressure assemblies. *Contributions to Mineralogy and Petrology* **142**, 640–652.

Wiebe, R. A. (1988). Structural and magmatic evolution of a magma chamber: The Newark Island Layered Intrusion, Nain, Labrador. *Journal of Petrology* **29**, 383–411.

Yu, Y. & Morse, S. A. (1992). Age and cooling history of the Kiglapait Intrusion from an 40Ar/39Ar study. *Geochimica et Cosmochimica Acta* **56**, 2471–2485.

APPENDIX A: NORM CALCULATION AND REDOX TREATMENT

Comparison of chemical compositions with modal data is easily made by use of the oxygen norm, convenient also for its treatment of variable Mg-ratios and for its similarity to the CIPW weight norm in the ternary space. An oxygen norm is calculated with the same routine as a cation norm, but with *oxygen equivalent molecular weights*, found by dividing the usual molecular weight by the number of oxygens in the formula of the constituent oxide, thus dividing by 2 for RO_2 oxides, by 3 for R_2O_3 oxides, by 1 for RO oxides, and by 5 for R_2O_5 oxides. The *oxygen number* is then found by dividing the weight percent of an oxide by the oxygen equivalent molecular weight, and the sum of the oxygen numbers for all constituents is taken for normalization of the oxygen units of the calculated normative minerals. Mineral formulas are combined according to the number of oxygens in the constituent oxides (e.g. Morse, 1994, p. 434). The remaining calculation proceeds as for the cation norm.

At least 97% of the compositional system considered here consists of olivine, augite and plagioclase (Table 1), so the phase relations among these three phases are well represented by an analog of the familiar ternary system Fo–Di–An (Osborn & Tait, 1952). The analogous end-members for the natural system projected to the ternary plane are olivine (OL), augite (AUG) and feldspar (FSP). The quantity of feldspar is unambiguously the sum of Or, An and Ab. However, the presence of Hy in the norm requires its appropriate allocation between augite and olivine. Whereas the standard CIPW convention forms *di* (represented as Di in the oxygen norm) at Wo = 50, the natural augite of the Kiglapait Intrusion near the base of the Upper Zone is of composition $Wo_{40}Hy_{10}$ (Morse & Ross, 2004). This composition can also be represented as $Di_{80}Hy_{20}$.

To form the AUG component, we first defined *hyaug* as the hypersthene component in augite, setting it equal to $0{\cdot}2di$. The rest of the adjustment was made with the following subroutine in TrueBasic.

```
SUB HYAUG
  let hyaug = 0·2*di
  if hyaug > hy then
  let hyaug = hy
  let hy = 0
    else if hyaug < hy then
    let hy = hy-hyaug
  end if
  let aug = (di + hyaug)/sum3
  !SUM3 = (OR + AB + AN + HY + OL + DI)/100
END SUB
```

Any remaining normative Hy was combined with Ol to make OLHY, as the mode of the Lower Zone contains only trivial amounts of hypersthene as rims on olivine, and the normative HY is assumed merely to represent minor excesses of SiO_2 in the analysis.

Redox treatment

Redox conditions within the graphite crucible at pressure and temperature are assumed from experience to reflect closely the initial composition of the charge over the short term. For the Lower Zone of the Kiglapait Intrusion, the initial redox and T–P conditions were considered reasonably well constrained to $\sim$2·5 kbar, 1250°C, and the WM buffer (Morse, 1980). With evolution of the liquid, the T–fO_2 trajectory tends toward the FMQ buffer, until titanomagnetite has crystallized after 86 PCS, when the fO_2 trend turns downward to more reducing conditions. In a fully realistic treatment of the Lower Zone LLD path, the melt compositions studied should reflect increased Fe–Ti oxide components as they evolve toward more augite-rich compositions. However, this evolution carries the risk of unwanted Fe enrichment of the charge, through complexing of carbon in the crucible with iron and phosphorus, as indeed found later (Peterson, 2000). For present purposes, it was expedient to minimize the effect of evolving ferric iron and Ti in the LLD by introducing only minor quantities of Fe–Ti oxide mineral and P to most of the bulk compositions. In a few runs, small beads of Fe–C melt were observed, so the run conditions are inferred to lie near or below the WM buffer.

The SMAR analyses (Table 1) and the redox evidence from Morse (1980) gave a best estimate of Fe_2O_3 in the liquid as a linear trend, given by $Fe_2O_3^L = 1{\cdot}04F_L^{-0{\cdot}622}$, where F_L is fraction liquid (Nolan & Morse, 1986). This

result implies an initial weight ferrous ratio FeO/(FeO + Fe_2O_3) = 0·9 (Fig. 2b), and, accordingly, we have referenced all our analyzed glass compositions to this ratio when calculating the oxygen norm. Our result is conditional upon this arbitrary assumption of the constant ratio.

The value chosen for the ferrous ratio has a small effect on the position of the plagioclase–olivine cotectic in the ternary plot. The more reduced the ferrous ratio, the more olivine (as fayalite) is generated in the norm, and the more the cotectic moves away from plagioclase toward olivine. For example, in composition KI BC2, (Table 2b) the calculated FSP value, normalized to the total of FSP + OLHY, varies by −0·82% when the ferrous ratio is changed from 0·85 to 0·95. The corresponding value of X_{Mg} changes from 0·56 to 0·51. The initial ferrous ratio for this sample, as made up, is 0·96; that for the composition KI BC96 is 0·95. Our LLD cotectic trace at more advanced, augite-rich stages, calculated at constant ferrous ratio, overestimates the OLHY content relative to FSP. The evolved end of the cotectic trace should be richer in feldspar than shown in our results, although probably not more than 1% richer.

APPENDIX B: LINEAR PARTITIONING IN BINARY SOLUTIONS

Linear partitioning occurs when a ratio of mole fractions is a linear function of composition in a binary solution. The ratio of mole fractions plotted is always chosen to be $\leq$1·0, and the composition plotted is always that of the phase appearing in the numerator. The resulting line runs from a constant, the exchange coefficient K_D, to 1·0.

Let the two binary components be denoted i and j and the two phases m and p. The general rule will be to assign i as the low-entropy (melting, vaporization) component, and m as the condensed (solid, liquid) phase. Then, the ratio of mole (atom, mass) fractions can be described as a partition coefficient D, akin to the Nernst distribution coefficient. Assuming ideal solution, we may write, for the mole fraction, $X_i = n_i/(n_i + n_j)$,

$$D_i \equiv X_i^m / X_i^p \leq 1{\cdot}0. \tag{B1}$$

And, likewise,

$$D_j \equiv X_j^m / X_j^p \geq 1{\cdot}0. \tag{B2}$$

At equilibrium, both the expressions above must be satisfied simultaneously. We now form

$$K_D \equiv (X_i/X_j)^m / (X_i/X_j)^p = D_i \cdot D_j^{-1}. \tag{B3}$$

If K_D is constant over the range of the binary solution and, hence, independent of T, then D_i is linear on X_i^m and anchored at K_D, 1·0, giving rise to the linear partitioning equation

$$D_i = K_D \cdot X_j^m + X_i^m \tag{B4}$$

derived elsewhere (Morse, 1996, 1997, 2000), and, conversely, D_j^{-1} is linear on X_j^p and anchored on the identical value of K_D, 1·0.

In application to plagioclase partitioning, let component i = Ab, j = An, phase m = solid, and $D = X_{Ab}^S / X_{Ab}^L$. The mole fractions are taken from the cation formula for the crystal and from the oxygen norm of the liquid. Then

$$D_{Ab} = K_D \cdot X_{An}^S + X_{Ab}^S. \tag{B5}$$

To retreive K_D from a known or assumed pair of phase compositions, we have

$$K_D = (D - X_{Ab}^S)/X_{An}^S. \tag{B6}$$

Hence, in the example cited in the text for the summation liquid compared with the plagioclase composition at 0 PCS:

$$X_{An}^S = 0{\cdot}67, \quad X_{Ab}^S = 0{\cdot}33 \text{ (Morse, 1979}a\text{, fig. 9)}$$

$$X_{An}^L = 0{\cdot}58, \quad X_{Ab}^L = 0{\cdot}42 \text{ (Table 1, column 4)}$$

$$\text{so } D = 0{\cdot}33/0{\cdot}42 = 0{\cdot}7857, \quad \text{and}$$
$$K_D = (0{\cdot}7857 - 0{\cdot}33)/0{\cdot}67 = 0{\cdot}68. \tag{B7}$$

By contrast, the estimated value of K_D extracted from the plagioclase variation of Morse (1979*a*, fig. 9) is ~0·5. A consensus result of K_D = 0·59 at 5 kbar is obtained from the HLCA composition of Fram & Longhi (1992, 0·646) and Grove *et al.* (1992, 0·534). From these results, a value of 0·54 was chosen for making up our experimental melt compositions. This was a lucky choice, as our first run (KI 1–1) gave crystals of composition An_{68}.

Any calculation of a binary loop within a multicomponent system involves approximations and algorithms, as found abundantly in, for example, Marsh *et al.* (1990), Grove *et al.* (1992) and Fram & Longhi (1992). The simple and classical CIPW convention, used here in the oxygen norm routine, assigns all Al after albite to the anorthite molecule, ignoring the fact that some Al resides in the augite component.

The present study is the first ever to use linear partitioning in the design of mixtures for melting and crystallization studies, and the first ever to return the experimental results to demonstrate and quantify the linear partitioning between plagioclase and melt.

Kiglapait run data for the KI Series (Sporleder, 1998)

Run	Composition	T (°C)	P (kb)	t (hrs)		Products	An	Fo
KI 1-1	KIBC96	1235	5	40		gl70, pl30	67.6	
1-2	KI3640 ac1					gl30, pl70	76.3	
1-3	KI3016a					gl100		
KI 4-1	KIBC96	1250	5	<6		gl100		
4-2	KI1110 ac1					gl100		
4-3	KI3016a					gl100		
KI 5-1	KIBC96	1220	5	25		gl+pl+ol		
5-2	KI3640 ac1					pl+ol		
5-3	KI3016a					gl+pl+ol		
KI 6a-1	KIBC96	1228	5	23.3		gl90, pl10	65.4	
6a-2	KI1110 ac1					gl20, pl70, ol10		
6a-3	KI3640 ac1					gl60, pl40, oltr		
6a-4	KI3016a					gl100		
KI 7-1	KIBC96	1228	4.67	24-36		gl25, pl60, ol15		
7-2	KI1110 ac1					pl80, ol20		
7-3	KI3640 ac1					pl80, ol20		
7-4	KI3016a					gl30, pl55, ol15		
KI 8-1	KI1110 ac1	1228	5	91.2		pl75, ol25		
8-2	KIBC96					gl5, pl60, ol35		
8-3	KI3640 ac1					pl75, ol25		
8-4	KI3016a					gl5, pl55, ol40		
KI 9-1	KIBC96	1246	4.75	91.2		gl70, pl30, oltr		
9-2	KI3016a					gl60, pl35, ol5		
9-3	KIBC962					gl60, pl30, ol10		
KI 10-1	KIBC96	1235	5	3		--		
10-2	KI1110 ac1					pl99, gltr		82.7
10-3	KIBC962					--		
10-4	KIBC963					--		
KI 12-1	KIBC962	1240	5	168		pl100		
12-2	KIBC963					pl100		
KI 14-1	KIBC2	1220	5	24		gl77, pl20, ol3	57.1	66.9
14-2	KI3016a					gl10, pl70, ol20		
14-3	KI1110 ac1					pl80, ol20		
KI 16-1	KIBC2	1230	5	7.5		gl80, pl20, oltr	62.3	71.9
16-2	KI3640 ac1					gl10, pl60, ol30		72.2
16-3	KI4845 ac1					pl50, ol50		74.1
KI 17-1	KIBC2	1235	5	17		gl100		
17-2	KI3640 ac1					gl45, pl40, ol5		
17-3	KI4845 ac1					gl20, pl60, ol20		

Run	Sample	T (°C)	P (kb)	t (hrs)		Products	An	Fo
KI 18-1	KI4845 ac1	1238	2	17		gltr, pl60, ol40		
18-2	KIBC22					gltr, pl70, ol30		
18-3	KI3016a3					pl75, ol25		
KI 20-1	KIBC3	1230	4.5	16.5		gl99, ol1		72.3
20-2	KIBC32					gl99, ol1		
20-3	KI1110 ac1					pl75, ol25		
KI 21-1	KIBC3	1220	4.5	16.5		gl20, pl50, ol30		
21-2	KIBC32					gl20, pl50, ol30		
21-3	KI4845 ac1					pl65, ol35		
KI 22-1	KIBC3	1225	4	16.5		gl40, pl50, ol10		
22-2	KIBC32					gl40, pl50, ol10		
22-3	KI4845 ac1					pl80, ol20		
KI 23-1	KIUZ1	1155	4	22.5		gl99, cpxtr		
23-2	KIUZ12					gl99, cpx1		
KI 24-1	KIUZ1	1145	4	17		gl35, pl40, oltr, cpx25		
24-2	KIUZ12					gl30, pl40, ol/cpx30		
KI 25-1	KIUZ1	1135	4.5	18		gl15, pl50, ol/cpx35		
25-2	KIUZ12					gl10, pl60, ol5, cpx25		
KI 26-1	KIUZ1	1125	5	18		gl94 pl3, ol3		
26-2	KIUZ12					gl89 pl5, ol6		
KI 27-1	KIUZ1	1160	5	7.5		gl100		
27-2	KIUZ13					gl100		
27-3	KI83PCS ac1					gl10 pl55, ol/cpx35	56.1	72.5
KI 28-1	KIUZ1	1150	5	7.5		gl91, pl2, cpx7		
28-2	KIUZ13					--		
28-3	KI83PCS ac1					--		63.7
KI 29-1	KIBC4b	1200	5	6.5		gl74, pl20, ol6		
29-2	KIBC4b2					gl79, pl15, ol6		
29-3	KI60PCS ac1					gl5,pl65, ol30		
KI 30-1	KIBC4b	1210	5	6		gl10,pl85, ol15		
30-2	KI60PCS ac1					gl90, pl10	60.0	
KI 31-1	KIUZ1	1150	5	6		gl88, pl2, cpx10	38.1	
31-2	KI83PCS ac1					pl60, ol15, cpx25		
KI 34-1	KIUZ2	1170	5	6		gl70, pl10, cpx20		
34-2	KI83PCS ac1					gl15, pl50, cpx35		
KI 35-1	KIUZ2	1190	5	6		gl100		
35-2	KI83PCS ac1					gl40, pl50, cpx10		
KI 36-1	KIUZ2	1180	5	6		gl99, cpx1		
36-2	KI83PCS ac1					gl40, pl50, ol10	51.3	62.6

Run	Sample	T (°C)	P (kb)	t (hrs)		Products	An	Fo
KI 37-1	KIUZ3	1180	5	6		gl94, pl5, cpx1	53.0	
37-2	KI60PCS ac1					gl5,pl65, ol30		
37-3	KI83PCS ac1					gl20,pl55, ol/cpx25		
KI 38-1	KIUZ4	1180	5	8		gl60, pl25, ol5		
38-2	KI60PCS					gl30, pl50, ol20		
38-3	KI60PCS ac1					gltr, pl70, ol30		
KI 39-1	KIUZ4	1195	5	7.5		gl89, pl10, ol1	55.6	
39-2	KI60PCS					gl75, pl20, ol5		
39-3	KI60PCS ac1					gl2, pl68, ol/cpx30		
KI 40-1	KIUZ4	1205	5	8		gl100		
40-2	KI60PCS					gl99, pl1	53.0	
40-3	KI60PCS ac1					gl40, pl40, ol20		
KI 41-1	KIUZ4	1200	5	8		gl100		
41-2	KI60PCS					gl95, pl5		
41-3	KI60PCS ac1					gl35, pl45, ol20		
KI 42-1	KIBC4b	1210	5	8.5		gl79, pl15, ol6	62.7	73.8
42-2	KI60PCS ac1					gl91, pl8, ol1		
42-3	KIBC4a					gl55, pl35, ol20		
KI 43-1	KIBC4b	1215	5	5.5		gl99, pl1		
43-2	KI60PCS ac1					gl60, pl30, ol10		
43-3	KIBC3					gl99, pl<1, ol1		
KI 44-1	KI50PCS	1215	5	8		gl99, pl1		
44-2	KI60acop1					gl25, pl45, ol30		
44-3	KI80acop1					gl15, pl45, ol20		
KI 45-1	KI50PCS	1210	5	6		gl80, pl20, ol<1		
45-2	KI60acop1					gl15, pl55, ol30		
45-3	KIBC3					gl65, pl25, ol10		
KI 46-1	KI60acop1	1205	5	8.5		gl10, pl60, ol30		
46-2	KI80acop1					gl15, pl55, ol30		
46-3	KIUZ4					gl100		
KI 47-1	KI60acop1	1200	5	6		gl5, pl65, ol30		
47-2	KI80acop1					gl15, pl55, ol30		
47-3	KIUZ4					gl99, pl1		
KI 48-1	KI60acop1	1190	5	8		gltr, pl70, ol30		
48-2	KI80acop1					gl2, pl68, ol30		
48-3	KIUZ4					gl80, pl20		
KI 53-1	New 50PCS	1205	5	2		gl96, pl3, ol<1		
53-2	KI70PCS					gl100		
53-3	Di9Ab91					gl6, pl85, di8		

Run	Sample	T (°C)	P (kb)	t (hrs)		Products	An	Fo
KI 56-1	KI50PCS4	1215	5	8		gl99, pl<1		
56-2	New 50PCS5	1205	5	2		gl96, pl3, ol<1		
KI 59-1	New 50PCS	1200	5	8		gl100		
59-2	KI70PCS					gl100		
59-3	Di9Ab91					sample lost		
KI 60-1	New 50PCS	1190	5	8		gl44, pl30, ol25, cpx<1		
60-2	KI70PCS					gl85, pl4, ol8, cpx 3		
60-3	UZ4					gl20, pl50, ol30		
KI 66-1	New 50PCS	1195	5	10		gl75, pl20, ol5		
66-2	KI70PCS					gl90, pl<<1, ol1, cpx9		
66-3	Di9Ab91					gl25, pl70, di5		

[1] Artificial cumulates designed to simulate ideal cumulates at a given stratigraphic level.

[2] Experimental compositions containing a plagioclase grain (An66, < 0.5 mm) added to study partitioning.

[3] Experimental compositions containing a plagioclase grain (An61, < 0.5 mm) added to study partitioning.

[4] Sample KI 50PCS from experiment KI 44-1, sectioned lengthwise to observe crystal distribution.

[5] Sample New 50PCS from experiment KI 53-1, sectioned lengthwise to observe crystal distribution.

Kiglapait run data for the 2K Series (Morse & Brady)

(Corrected temperatures in italics)

Run No.	Composition	T	P	t	OP	Gl	Pl	Ol	Aug
	UNITS:	°C	kb	hr	%	%	%	%	%
2K-1-3	Failed runs								
2K-4.1	KIBC96	1235	5	46		40	52	8	0
2K-4.2	KI3016a					60	30	8	Op2
2K-4.3	KIBC3					60	30	10	
2K-5.1	KIBC96	1245	5	5		99+	tr		
2K-5.2	KI3016a					100			
2K-5.3	HN7201Sa					0	Sanidine		
2K-6.1	KIBC96	1240	5	45		60	35	5	
2K-6.2	KI3016a					70	x	x	
2K-6.3	KIBC3					67	25	8	
2K-7.1	KIBC96	1242	5	3.3		85	15		
2K-7.2	KI3016a					99?			tr
2K-7.3	KIBC3					100			
2K-8.1	N50PCS	1210	5	2.7	68	100			
2K-8.2	60PCS	*1211*				100			
2K-8.3	N70 = 78					100			
2K-9.1	N50PCS	1195	5	8.5		100			
2K-9.1	60PCS	*1210*				95	5		
2K-9.1	N70 = 78					100			
2K-10.1	N50PCS	1185	5	3.8		100			
2K-10.1	60PCS	*1211*				99+	tr		
2K-10.1	N70 = 78					100			
2K-11.1	N50PCS	1175	5	3		50+	45	15	
2K-11.2	60PCS	*1194*				30	50	20	
2K-11.3	N70 = 78	*1194*				60	20	8	12
2K-12.1	N50PCS	1190	5	3		60	30	10	
2K-12.2	N7078+OL	*1199*				97	3		
2K-12.3	N70=78					96	4		
2K-13.1	FAIL								
2K-14.1	N50	1188	5	24		40	40	20	
2K-14.2	78+3OL	*1193*				71	20	6	3
2K-14.3	78PCS					64	30	6	2
2K-15.1	R50PCS	1230	5	2.8		>99	0	tr	
2K-15.2	R65PCS					100			
2K-15.3	R75PCS					100			
2K-16.1	R50PCS	1210	5	3		95	0	5	
2K-16.2	R65PCS					100			
2K-16.3	R75PCS					100			
2K-17.1	R50a	1220	5	2.8		>99	0	tr	
2K-17.2	R65a					100			
2K-17.3	R75a					100			
2K-18.1	R50a	1200	5	3		60	28	12	
2K-18.2	R65a					<90	7	3	
2K-18.3	R75a					100			
2K-19.1	R50a	1210	5	2.8		80	14	6	
2K-19.2	R65a					100		tr	
2K-19.3	R75a					100			

Run No.	Composition	T	P	t	OP	Gl	Pl	Ol	Aug
	UNITS:	°C	kb	hr	%	%	%	%	%
2K-20.1	SanMar01	1260	5	3		50	Sanidine		
2K-20.2	KI4845ac					15	55	30	
2K-20.3	KI3640ac					35	20	45	
2K-21.1	R50a	1217	5	9.1		97	2	1	
2K-21.2	R50a	Note: run with eutectoid texture							
2K-21.3	R50a								
2K-22	FAIL								
2K-23	R65aFAIL								
2K-24	3x R65a	1205	5	3		100			
2K-25.1	R65a	1202	5	3		100			
2K-25.2	R65a					100			
2K-25.3	Unk#3								
2K-26.1	R75a	1190	5	3		100			
2K-26.2	R75aOL					100			
2K-26.3	UZ3OL					100			
2K-27.1	R75a	1180	5	3		100			
2K-27.2	R75aOL					98		2	
2K-27.3	UZ3OL					100			
2K-28.1	R75a	1170	5	3		80	15	5	
2K-28.2	R75aOL	*1191*				81	12	7	
2K-28.3	UZ3OL					75	15		10
2K-29	R65a	1190	5	3	all	100			
2K-30.1	R75a	1177	5	3		100			
2K-30.2	R65a					100	tr		
2K-30.3	ILP-1					5	65	Il	30
2K-31	FAIL								
2K-32	FAIL								
2K-33	FAIL								
2K-34.1	ILP1	1173	5	3		ILP	System IL-PL		
2K-34.2	ILP2	1173	5	3		ILP			
2K-34.3	R65a					100			
2K-35	FAIL								
2K-36.1	ILP1	1160	5	3	66	40	35		Ilm
2K-36.2	R65a	T>>				100			
2K-36.3	R75a					100			
2K-37.1	R50a	1160	5	3		0	x	x	New
2K-37.2	R65a					0	x	x	x
2K-37.3	R75a					0	x	x	x
2K-38.1	R50a	1200	5	3		70	20	10	
2K-38.2	R65a					85	10	5	
2K-38.3	R75a					100			
2K-39.1	R65a	1205	5	3	def	70			
2K-39.2	N50PCS	*1194*				60			
2K-39.3	60PCS					30			
2K-40.1	R65a	1210	5	3	72	96	3	1	
2K-40.2	N50PCS	*1207*				98	2		sulf
2K-40.3	60PCS					83	15	2	?
2K-41.1	60PCS	1195	5	3		40	45	5	10
2K-41.2	R75a	*1196*				88	9	3	
2K-41.3	78PCS					70	20	4	6

Run No.	Composition	T	P	t	OP	Gl	Pl	Ol	Aug
	UNITS:	°C	kb	hr	%	%	%	%	%
2K-42.1	60PCS	1200	5	3	68+	98	2		
2K-42.2	R75a	*1210*				100			
2K-42.3	78PCS					100			
2K-43.1	60PCS	1200	5	3	67	50	40	8	
2K-43.2	R75a	*1199*				90	7	3	tr
2K-43.3	78PCS					82	12	4	2
2K-44.1	60PCS	1205	5	3	63	67	25	8	
2K-44.2	R75a	*1203*				98	2	tr	
2K-44.3	78PCS					<96	3	1	0.5
2K-45.1	KIUZ3	1200	5	3	<63	96	3	1	
2K-45.2	KIUZ4	*1205*				93	5		2
2K-45.3	60PCS					75	20	5	
2K-46.1	KIBC96	1235	5	3	<67	65	34	1	
2K-46.2	KIBC2					74	22	4	
2K-46.3	KIBC3					60	30	10	
2K-47.1	KIBC96	1245	5	3	<70	75	25		
2K-47.2	KIBC2	*1240*				95	5	tr	
2K-47.3	KIBC3					98	2	tr	
2K-48.1	KIBC96	1250	5	3	<69	>99	<1		
2K-48.2	KIBC2					100			
2K-48.3	KIBC3					100			
Notes: OP, Output Power. tr, trace. Percentages are visual estimates.									
29 April 2002									
19 July 2002									
15-Apr-04									